 doi:10.20944/preprints202011.0616.v1

Article

In Silico Assessment of Class I Antiarrhythmic Drugs Effects on Pitx2-induced Atrial Fibrillation: Insights from Populations of Electrophysiological Models of Human Atrial Cells and Tissues

Jieyun Bai [1,#*], Yijie Zhu [1,#], Andy Lo [2], Meng Gao [3,*], Yaosheng Lu [1], Jichao Zhao [2] and Henggui Zhang [4]

[1] Department of Electronic Engineering, College of Information Science and Technology, Jinan University, Guangzhou, 510632, China; bai_jieyun@126.com (J.B.); 584314899@qq.com (Y.Z.); tluys@jnu.edu.cn (Y.L.)
[2] Auckland Bioengineering Institute, University of Auckland, Auckland, 1010, New Zealand; alo006@auckland.ac.nz (A.L.); j.zhao@auckland.ac.nz (J.Z.)
[3] Department of Computer Science and Technology, College of Electrical Engineering and Information, Northeast Agricultural University, Harbin, 150030, China; gaomeng@neau.edu.cn
[4] Biological Physics Group, School of Physics & Astronomy, The University of Manchester, Manchester, M13 9PL, United Kingdom; henggui.zhang@manchester.ac.uk
[#] J.B. and Y.Z. contributed equally to this work.
[*] Correspondence: bai_jieyun@126.com; Tel.: +86-1327-461-8376 (J.B.) or gaomeng@neau.edu.cn; Tel.: +86-1577-676-8916 (M.G.)

Abstract: Electrical remodelling as a result of the homeodomain transcription factor 2 (Pitx2)-dependent gene regulation was linked to atrial fibrillation (AF) and AF patients with single nucleotide polymorphisms at chromosome 4q25 responded favorably to Class I antiarrhythmic drugs (AADs). The possible reasons behind this remain elusive. The purpose of this study was to assess the efficacy of AADs disopyramide, quinidine, and propafenone on human atrial arrhythmias mediated by Pitx2-induced remodelling, from a single cell to the tissue level, using drug binding models with multi-channel pharmacology. Experimentally calibrated populations of human atrial action potential (AP) models in both sinus rhythm (SR) and Pitx2-induced AF conditions were constructed by using two distinct models to represent morphological subtypes of AP. Multi-channel pharmacological effects of disopyramide, quinidine, and propafenone were considered. Simulated results showed that Pitx2-induced remodelling increased maximum upstroke velocity ($dVdt_{max}$) and conduction velocity (*CV*), and decreased AP duration (*APD*) and wavelength (*WL*). At the concentrations tested in this study, these AADs decreased $dVdt_{max}$ and *CV* and prolonged *APD* in the setting of Pitx2-induced AF. Our findings of alterations in *WL* indicated that quinidine and disopyramide may be more effective against Pitx2-induced AF by prolonging *WL*.

Keywords: action potential; atrial fibrillation; in silico model; population of models; Class I antiarrhythmic drugs; flecainide; disopyramide; quinidine; propafenone; Pitx2

1. Introduction

Although atrial fibrillation (AF) incidence increases with age, and with the context of concomitant cardiac pathologies [1], population-based genome-wide association studies (GWAS) showed that one-third of AF patients carry common genetic variants, suggesting that AF has a heritable component [2]. Recently, many AF-associated loci were identified in GWAS [3-9] and the most common AF susceptibility locus firstly identified in European, Chinese and Japanese populations is located on chromosome 4q25 [10]. The gene-poor 4q25 region harbors the paired-like

homeodomain transcription factor 2 (Pitx2), which has been fundamentally linked to AF [11-20] although the basis for this connection remains obscure. In early cardiac embryogenesis, Pitx2 suppresses left atrial automaticity and formation of "sinus node-like structures" in the left atrium [21] and contributes to the formation of the pulmonary vein myocardium [13]. In the adult heart, Pitx2 is mainly expressed in the left atrium and pulmonary vein [11]. Experimental studies of Pitx2-induced AF have indicated that downregulation of Pitx2 creates a predisposition to AF without marked structural changes in the atria [11, 15, 18, 22] via shortened atrial repolarization [22], a more depolarized resting membrane potential (RMP) [18] and abnormalities in calcium cycling [17, 23, 24]. Gene expression analyses highlighted that Pitx2 regulated genes of ion channels [11, 12, 17, 22, 23, 25, 26] in a dose-dependent manner. Based on these experimental data on changes in expression of ion channels, we constructed multi-scale models of human atrial electrophysiology to investigate mechanisms by which Pitx2-induced remodelling promotes AF in our previous studies [27-33]. However, effective management of AF remains a challenge, and is incompletely understood in the context of Pitx2-induced AF.

A population-based study assessed the influence of AF-associated loci on the response to antiarrhythmic drug (AAD) therapies and showed that carriers of the variant allele at rs10033646 on chromosome 4q25 (Pitx2) responded favorably to Class I AADs [34]. Class I AADs used in AF include flecainide, disopyramide, quinidine and propafenone [35]. The pharmacological effects of flecainide in Pitx2-induced AF were investigated by using a multi-scale computational model and simulated results demonstrated that flecainide is effective for the treatment of Pitx2-induced AF patients by preventing spontaneous calcium release [36]. However, the efficacy of other Class I AADs disopyramide, quinidine, and propafenone on human atrial arrhythmias mediated by Pitx2-induced remodelling remains elusive.

Although the efficacy of disopyramide, quinidine, and propafenone on human atrial patho-electrophysiology associated with hERG-linked short QT syndrome has been investigated using a multi-scale computational model [37], mechanisms by which short QT mutations promote AF may be different from that underlying Pitx2-induced AF [27-32, 36]. Also, both clinical [34] and theoretical [36] studies of pharmacotherapy for Pitx2-induced AF often ignored inter-subject variability in atrial electrophysiology properties. Population-based computational approaches that can capture key disease conditions have proven valuable for understanding inter-subject variability in electrophysiological properties [38-40] and cardiotoxicity [41-53]. Similarly, these methods were useful in AF [54-58]. Recently, a novel Quantitative Systems Pharmacology Framework was prospered based on these population-based computational modelling and effects of multi-atrial-predominant potassium-current block in AF were investigated [55].

Here, following the Quantitative Systems Pharmacology Framework developed by Ni et al. [55], we constructed populations of in silico models calibrated to values of action potential (AP) biomarkers reported in an experimental dataset on AP recordings [59]. Using these experimentally calibrated models, we simulated and assessed actions of Class I AADs on human atrial electrophysiology. AP duration (*APD*) and maximum upstroke velocity ($dVdt_{max}$) were quantified to evaluate anti-AF effects of Class I AADs on AP at the cellular level, while conduction velocity (*CV*) and wavelength (*WL)* were quantified to assess the effects of Class I AADs on AP propagation at the tissue level. Sensitivity analyses of AP biomarkers were applied to understand the ionic mechanisms underlying Pitx2-induced AF and the efficacy of these AADs. Finally, we performed population-based simulations of Pitx2-induced remodelling and predicted a reduction in *APD* and *WL* and an increase in *CV* and $dVdt_{max}$. Further simulations of actions of Class I AADs on Pitx2-induced AF exhibited *APD* prolongation and a reduction in *CV* and $dVdt_{max}$. Our results showed that quinidine and disopyramide led to *WL* prolongation compared to the drug-free AF conditions, but propafenone caused *WL* shortening. These findings suggest that quinidine and disopyramide may be effective against Pitx2-induced AF.

Preprints (www.preprints.org) | NOT PEER-REVIEWED | Posted: 24 November 2020 doi:10.20944/preprints202011.0616.v1

2. Results

2.1 Overview of in silico assessment of Class I antiarrhythmic drugs

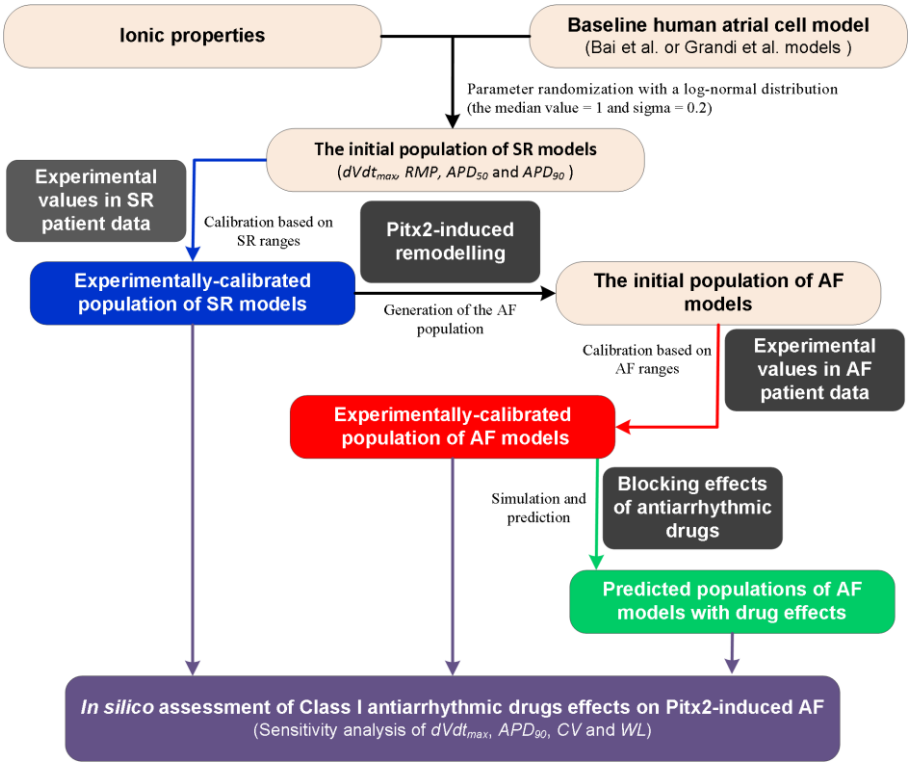

Figure 1. Flow chart illustrating the process for in silico assessment of Class I antiarrhythmic drugs effects on Pitx2-induced atrial fibrillation (AF). Note: There are two distinct morphological subtypes of human atrial action potential (AP) [59] and thereby the Bai et al. model with a notch-and-dome AP morphology [27] and the Grandi et al. model with a triangular AP shape [60] were used in the present study. Class I antiarrhythmic drugs assessed include quinidine, disopyramide and propafenone. Abbreviations: Pitx2-The homeodomain transcription factor 2, SR-Sinus rhythm; $dVdt_{max}$-Maximum upstroke velocity, *RMP*-Resting membrane potential, APD_{50} and APD_{90}-AP duration at 50% and 90%, respectively, *CV*-Conduction velocity and *WL*-Wavelength.

Table 1. Parameters associated with ionic properties for constructing populations of atrial models.

Parameters	Definition	Models	
		Bai *et al.* [27]	Grandi *et al.* [60]
G_{Na}	Maximal I_{Na} conductance	√	√
G_{Ks}	Maximal I_{Ks} conductance	√	√
G_{K1}	Maximal I_{K1} conductance	√	√
G_{CaL}	Maximal I_{CaL} conductance	√	√
G_{to}	Maximal I_{to} conductance	√	√
G_{Kr}	Maximal I_{Kr} conductance	√	√
G_{Ncx}	Maximal I_{Ncx}	√	√
G_{BNa}	Maximal I_{BNa} conductance	√	√
G_{BCa}	Maximal I_{BCa} conductance	√	√
G_{Nak}	Maximal I_{Nak}	√	√
G_{PCa}	Maximal I_{PCa} conductance	√	√
G_{PK}	Maximal I_{PK} conductance	√	√
G_{Kur}	Maximal I_{Kur} conductance	√	√
G_{rel}	Maximal I_{rel} via *RyR*	√	√
G_{up}	Maximal I_{up} via *SERCA*	√	√
G_{CaNa}	Maximal I_{CaNa} conductance	*N/A*	√
G_{CaK}	Maximal I_{CaK} conductance	*N/A*	√
G_{ClCa}	Maximal I_{ClCa} conductance	*N/A*	√
G_{BCl}	Maximal I_{BCl} conductance	*N/A*	√
G_{NaL}	Maximal I_{NaL} conductance	*N/A*	√

Preprints (www.preprints.org) | NOT PEER-REVIEWED | Posted: 24 November 2020 doi:10.20944/preprints202011.0616.v1

Table 2. Experimental data on AP biomarkers [59] under atrial fibrillation (AF) and sinus rhythm (SR) conditions.

Biomarkers	SR (n = 238)	AF (n = 214)
APD_{90} (ms)	317.41 ± 43.19	217.45 ± 35.74
APD_{50} (ms)	138.09 ± 45.14	100.41 ± 6.31
RMP (mV)	-73.98 ± 0.86	-76.85 ± 0.83
$dVdt_{max}$(V/s)	219.44 ± 14.65	231.56 ± 16.51

Note: Values are presented in mean ± standard error. AP biomarkers include APD_{50}, APD_{90}, *RMP* and $dVdt_{max}$. Abbreviations: $dVdt_{max}$-Maximum upstroke velocity, *RMP*-Resting membrane potential, and APD_{50} and APD_{90}-AP duration at 50% and 90%, respectively.

Table 3. Parameters associated with Pitx2-induced remodelling.

Experimental observation	Parameters	Changes (%)
-60% (SCN5A & SCN1B) [22] -40% (SCN5A & SCN1B) [25] +95% SCN5A [17] No Change [18] +70-90% (SCN1B) [61]	G_{Na}	+10%
+500% CACNA1D [12] -50% CACNA1C [26] -30% CACNA1C [25] Decreased CACNA1C [11]	G_{CaL}	+30%
+150% (KCNQ1) [26] Increased voltage-dependent potassium current [11] +80% (KCNQ1) [61] +50-70% (KCNQ1) [15]	G_{Ks}	+150%
-20% (KCNJ2 & KCNJ12) [22] +30 (KCNJ2 & KCNJ12) [25] -25% KCNK5 [18]	G_{K1}	-30%
+145% RyR2 [12] +30% RyR2 [23] +30% RyR2 [25] +10% RyR2 [17]	G_{rel}	+100%
+50% ATP2A2 [12] +1000% ATP2A2 [23] +100% ATP2A2 [25] +12% ATP2A2 [17] +37% SERCA2 [24]	G_{up}	+30%

Note: We assumed that changes in mRNA expression are quantitatively reflected at the final functional level of ion channels. Parameters associated with Pitx2-induced remodelling of ion channels include G_{Na}, G_{CaL}, G_{Ks}, G_{K1}, G_{rel}, and G_{up}.

A flow chart illustrating the process for in silico assessment of Class I AADs effects on Pitx2-induced AF is presented in **Figure 1.** First, the initial population of sinus rhythm (SR) models was created by randomly perturbing parameters associated with ionic properties (**Table 1**) of the baseline human atrial cell models [41]. The Bai et al. model displaying a type-1 AP with notch-and-dome morphology [27] and the Grandi et al. model displaying a type-3 AP with typical triangular shape [60] were chosen as the baseline human atrial cell models to represent distinct morphological subtypes of human atrial AP [62]. Parameters associated with ionic properties were allowed to vary independently according to a log-normal distribution and sigma was set to be 0.2 to cover a range of variability similar to that seen in experiments based on previous studies [41, 55, 63, 64]. Second, we used the initial models to simulate human atrial AP by considering stimulation frequency (1Hz) under the experimental conditions [59] and calculate AP biomarkers of each initial model. The initial models generated in the previous step were selected to constitute the SR population whose simulated

 doi:10.20944/preprints202011.0616.v1

electrophysiological properties are in range with the same properties in experimental data on AP biomarkers (including $dVdt_{max}$, *RMP*, APD_{50} and APD_{90}) in **Table 2**. This step yields the experimentally-calibrated population of SR models [54]. Third, electrical remodelling due to impair Pitx2 (**Table 3**) was introduced into SR model variants to generate the initial population of AF models. Fourth, we used experimental AP biomarkers to calibrate the AF population by excluding the model variants in which values of simulated biomarkers were outside the experimentally observed range (**Table 3**) reported by Ravens et al [59]. Fifth, the blocking effects of AADs on ion channels (**Table 4**) were incorporated into experimentally-calibrated Pitx2-induced AF models to evaluate their effects on the virtual atrial myocytes. Finally, sensitivity analyses [41, 55] of $dVdt_{max}$ and APD_{90} at the cellular level and *CV* and *WL* at the tissue level were applied to understand modulations by ionic parameters of Pitx2-induced remdoelling and ion channels affected by AADs. On the basis of model responses, AADs that eliminates the arrhythmogenic propensity of the atrial substrate arising from Pitx2-induced remodelling were selected.

Table 4. Parameters associated with blocking effects of antiarrhythmic drugs.

Currents	Disopyramide			Quinidine			Propafenone		
	IC_{50}(μM)	*nH*	Ref.	IC_{50}(μM)	*nH*	Ref.	IC_{50}(μM)	*nH*	Ref.
I_{Na}	168.4	1.09	[65]	14.6	1.22	[65]	1.2	1.0	[66]
I_{CaL}	1036.7	1.0	[65]	14.9	1.0	[67]	1.7	1.0	[68]
I_{to}	20.9	1.0	[69]	21.8	1.0	[70]	4.8	1.0	[71]
I_{Ks}	88.1	1.0	[72]	44.0	1.0	[73]	-	-	-
I_{Kr}	14.4	0.91	[65]	0.72	1.06	[65]	2.0	1.0	[74]
I_{Kur}	25.0	1.0	[75]	6.6	1.0	[70]	4.4	1.0	[76]
I_{K1}	-	-	-	42.6	1.0	[70]	16.8	1.0	[77]

Note: Antiarrhythmic drugs investigated include disopyramide, quinidine and propafenone. Ion currents associated with these drugs included I_{Na}, I_{CaL}, I_{to}, I_{Ks}, I_{Kr}, I_{Kur} and I_{K1}. Blocking effects of drugs on ion currents were modelled with the half-maximal inhibitory concentration (IC_{50}) and Hill-coefficient (*nH*) value. IC_{50} and *nH* were extracted from the literature.

Table 5. AP biomarkers obtained from the Bai et al. model and the Grandi et al. model under atrial fibrillation (AF) and sinus rhythm (SR) conditions.

Biomarkers	Bai *et al.* model		Grandi *et al.* model	
	SR (n = 238)	AF (n = 214)	SR (n = 153)	AF (n = 79)
APD_{90} (ms)	254.57 ± 41.51	187.83 ± 25.56	261.84 ± 58.49	236.52 ± 42.76
APD_{50} (ms)	191.71 ± 32.19	125.16 ± 22.89	59.78 ± 26.39	49.29 ± 16.45
RMP (mV)	-79.94 ± 3.29	-79.38 ± 3.30	-81.00 ± 0.22	-81.03 ± 0.31
$dVdt_{max}$(V/s)	192.82 ± 81.23	210.72 ± 86.83	353.19 ± 50.01	367.42 ± 48.68

Note: Values are presented in mean ± standard error. AP biomarkers include APD_{50}, APD_{90}, *RMP* and $dVdt_{max}$. Abbreviations: $dVdt_{max}$-Maximum upstroke velocity, *RMP*-Resting membrane potential, and APD_{50} and APD_{90}-AP duration at 50% and 90%, respectively.

2.2 The experimentally-calibrated populations of human atrial myocytes under SR and AF conditions

Representing a type-1 AP with notch-and-dome morphology, the Bai et al. model [27] was used to generate the initial SR population of human atrial cell model variants. According to the physiological range of AP biomarkers ($dVdt_{max}$, *RMP*, APD_{50} and APD_{90} values at 1Hz pacing) measured experimentally (**Table 2**), populations of 610 SR models out of the initial pool of 1,200 models were selected to generate the experimentally-calibrated population of SR models. Next, we incorporated Pitx2-induced electrical remodelling (**Table 3**) into the SR population of 610 variants to generate the initial AF population, and then calibrated this AF population to the experimentally measured AP biomarkers (**Table 2**). Representative AP traces for the experimentally-calibrated SR population of 610 models and AF population of 214 models, respectively, are shown in **Figure 2a** and **Figure 2b**. Distributions of AP biomarkers of the experimentally-calibrated SR models are compared to that of AF models (**Figure 2c-d**). In detail (**Table 5**), $dVdt_{max}$ is increased from 192.82 ± 81.23 V/s for

Preprints (www.preprints.org) | NOT PEER-REVIEWED | Posted: 24 November 2020 doi:10.20944/preprints202011.0616.v1

the SR condition to 210.72 ± 86.83 V/s for the AF condition, whereas APD_{90} (187.83 ± 25.56 ms vs. 254.57 ± 41.51 ms) and APD_{50} (125.16 ± 22.89 ms vs. 191.71 ± 32.19 ms) were abbreviated due to Pitx2-induced remodelling. No significant changes in *RMP* (-79.38 ± 3.30 mV vs.-79.94 ± 3.29 mV) are observed.

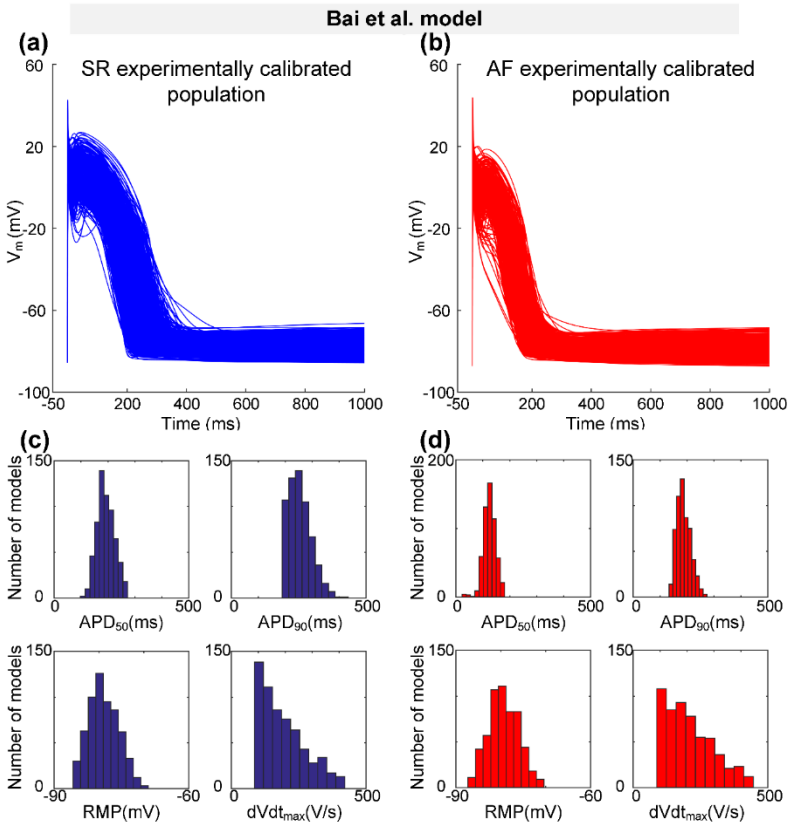

Figure 2. The experimentally-calibrated populations constructed with the Bai et al. model for sinus rhythm (SR) and atrial fibrillation (AF) conditions. **a-b**, Representative traces of action potential (AP) models in SR and Pitx2-induced AF conditions. **c-d,** Distributions of AP biomarkers (including $dVdt_{max}$, *RMP*, APD_{50} and APD_{90}) under SR and Pitx2-induced AF conditions.

Representing a type-3 AP with a typical triangular shape, the Grandi et al. model [60] was also used to generate the experimentally-calibrated populations according to the physiological range of AP biomarkers [59] measured experimentally (**Table 2**). 153 SR models and 79 AF models were selected to constitute the SR population and the AF population, respectively. **Figure 3** shows representative AP traces (**Figure 3a-b**) and distributions of AP biomarkers (**Figure 3c-d**) for the SR population and the AF population. Consistent with changes in AP biomarkers observed in the Bai et al. model (**Figure 2c-d** and **Table 5**), especially, $dVdt_{max}$ is increased from 353.19 ± 50.01 V/s for the SR population to 367.42 ± 48.68 V/s for the AF population, whereas APD_{90} is decreased from 261.84 ± 58.49 ms for the SR population to 236.52 ± 42.76 ms for the AF population (**Table 5**).

Preprints (www.preprints.org) | NOT PEER-REVIEWED | Posted: 24 November 2020 doi:10.20944/preprints202011.0616.v1

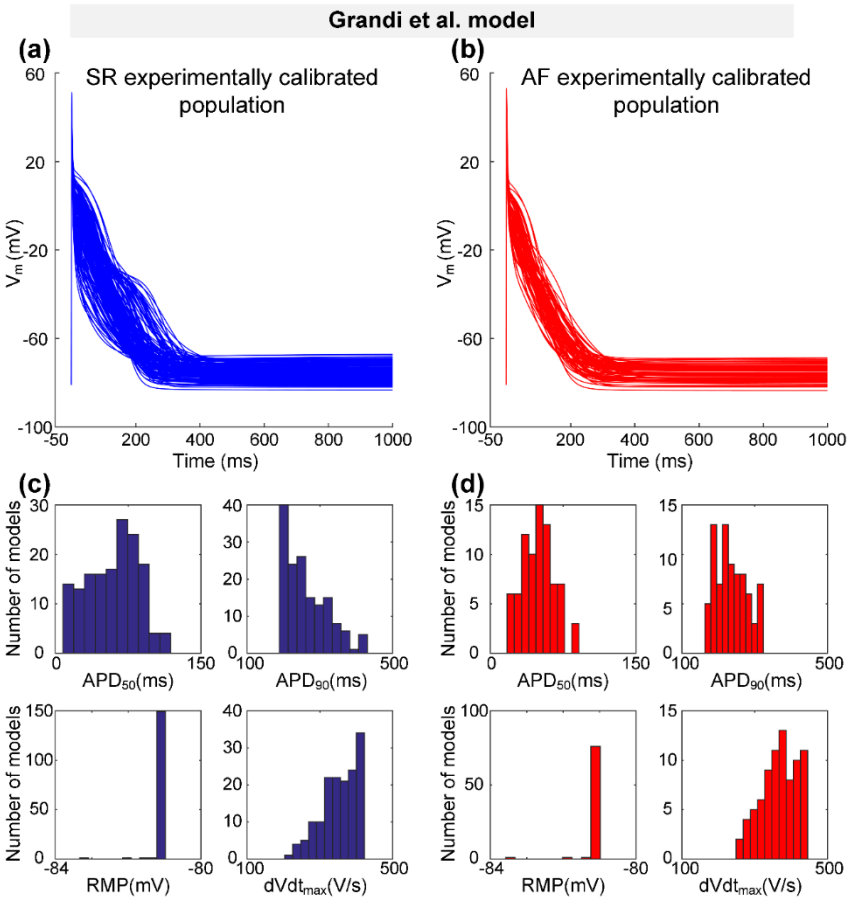

Figure 3. The experimentally-calibrated populations constructed with the Grandi et al. model for sinus rhythm (SR) and atrial fibrillation (AF) conditions. **a-b**, Representative traces of action potential (AP) models in SR and Pitx2-induced AF conditions. **c-d**, Distributions of AP biomarkers (including $dVdt_{max}$, *RMP*, APD_{50} and APD_{90}) under SR and Pitx2-induced AF conditions.

2.3 Sensitivity analysis revealed alterations in depolarization and repolarization of AP

Experimental studies have demonstrated that sensitivity analyses of $dVdt_{max}$ and APD_{90} can provide insights into alterations in the depolarization rate [78-81] and the repolarization time [82] of the cardiac tissue. We applied partial correlation analysis to predict alterations in $dVdt_{max}$ and APD_{90} when electrical remodelling (listed in **Table 3**) due to impaired Pitx2 was introduced or ion channels (listed in **Table 4**) were blocked by Class I AADs. Parameters associated with Pitx2-induced electrical remodelling include G_{Na}, G_{CaL}, G_{Ks}, G_{K1}, G_{rel} and G_{up}, while parameters affected by actions of AADs (including disopyramide, quinidine and propafenone) include G_{Na}, G_{CaL}, G_{to}, G_{Ks}, G_{Kr}, G_{Kur} and G_{K1}. We used partial correlation analysis to calculate partial correlation coefficients (PCCs) to quantify correlations between the parameter values and $dVdt_{max}$ and APD_{90}, respectively. In **Figure 4a-d**, $dVdt_{max}$ PPCs are positive for G_{Na} in Bai et al. and Grandi et al. populations, suggesting that upregulated I_{Na} in Pitx2-induced remodelling would tend to increase depolarization rate and inhibiting I_{Na} due to actions of AADs favors to reduce depolarization rate. In **Figure 4e-h**, APD_{90} PPCs are negative for G_{Ks}, G_{Kr} and G_{K1} but not for G_{CaL}, indicating that upregulated G_{Ks} and downregulated G_{CaL} in Pitx2-induced remodelling cause APD shortening and block of these potassium currents (i.e., I_{Ks}, I_{Kr} and I_{K1}) would tend to prolong APD. APD_{90} PPCs for G_{to} and G_{Kur} are also negative in Grandi et al. but not Bai et al. population. Therefore, in Grandi et al. populations, APD_{90} PPCs for G_{to}, G_{Ks}, G_{Kr}, G_{Kur} and G_{K1} are negative, suggesting that inhibiting these currents due to actions of AADs produces positive APD prolongation. In contrast, in Bai et al. populations, negative APD_{90} PPCs are seen for I_{Ks}, I_{Kr} and I_{K1} only, indicating that the block effects of Class I drugs on I_{Ks}, I_{Kr} and I_{K1} are associated with positive APD prolongation, but the block effects of AADs on G_{to} and G_{Kur} with negative APD prolongation. In

Preprints (www.preprints.org) | NOT PEER-REVIEWED | Posted: 24 November 2020 doi:10.20944/preprints202011.0616.v1

addition, PPCs of APD_{90} and $dVdt_{max}$ for other ionic properties (listed in **Table 1**) are shown in **Figure 1S** and **Figure 2S** in the Supplementary Material.

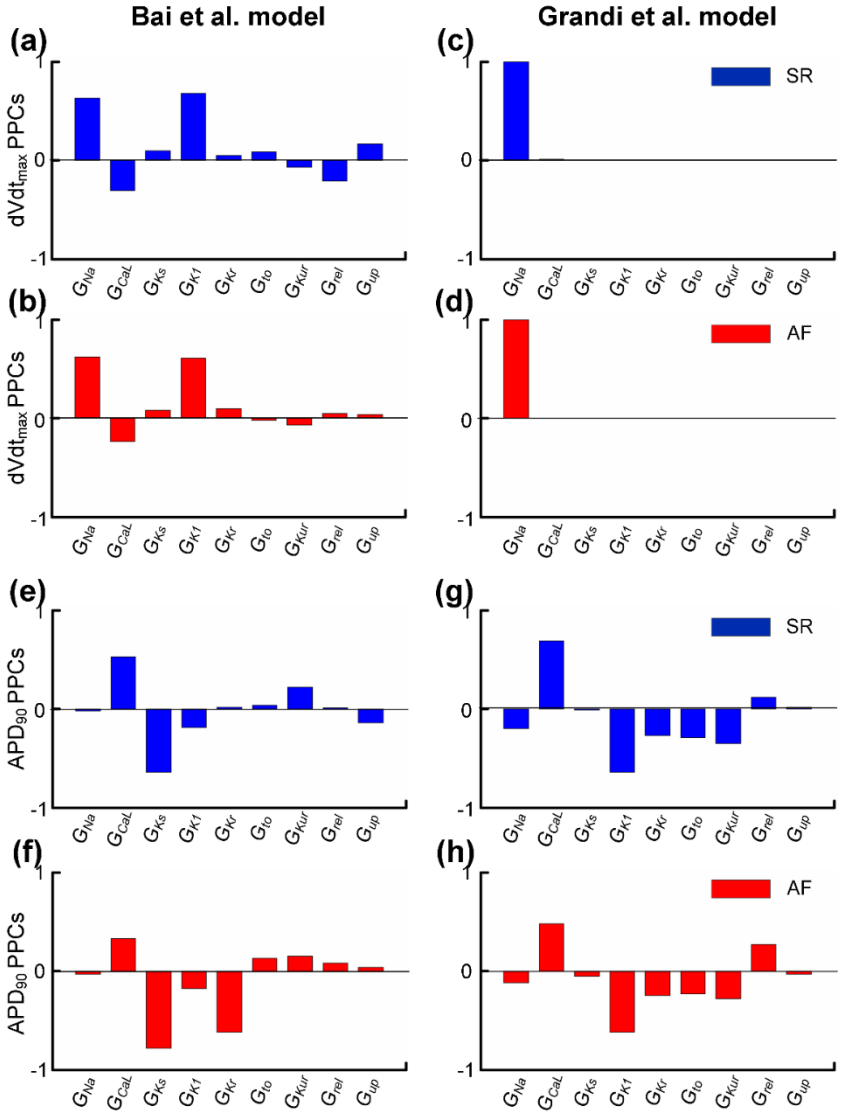

Figure 4. Partial correlation coefficients (PPCs) between biomarkers ($dVdt_{max}$ or APD_{90}) and parameters associated with Pitx2-induced electrical remodelling (G_{Na}, G_{CaL}, G_{Ks}, G_{K1}, G_{rel} and G_{up}) or actions (G_{Na}, G_{CaL}, G_{to}, G_{Ks}, G_{Kr}, G_{Kur} and G_{K1}) of antiarrhythmic drugs. PPCs between $dVdt_{max}$ and G_{Na}, G_{CaL}, G_{Ks}, G_{K1}, G_{Kr}, G_{to}, G_{Kur}, G_{rel} or G_{up} for the virtual atrial myocytes created by the Bai et al. model in SR (**a**) and AF (**b**) are compared to that for virtual atrial myocytes in the SR (**c**) and AF (**d**) populations created by the Grandi et al. model. PPCs of APD_{90} for virtual atrial SR (**e**) and AF (**f**) myocyte populations created the Bai et al. model are compared to that for the virtual atrial myocytes created by the Grandi et al. model in SR (**g**) and AF (**h**).

2.4 Antiarrhythmic effects of Class I drugs on $dVdt_{max}$ and APD_{90} at the cellular level

According to experimental data on actions of Class I AADs on ion currents, their effects were incorporated into experimentally-calibrated models in the AF population created with the Bai et al. model. Parameters associated with the effects of AADs were G_{Na}, G_{CaL}, G_{to}, G_{Ks}, G_{Kr}, G_{Kur} and G_{K1} (**Table 4**). Class I AADs investigated here included disopyramide, quinidine and propafenone. Taking into account plasma protein binding, estimates of the most likely unbound concentrations of propafenone, disopyramide and quinidine have been given as ~0.15-1 μM [83-85], 1 μM and 2 μM [86], respectively. To encompass likely total as well as unbound concentrations, we selected to simulate effects of a wide range of concentration of propafenone (low dose Prop_L: 0.2, medium dose Prop_M: 0.5 and high

Preprints (www.preprints.org) | NOT PEER-REVIEWED | Posted: 24 November 2020 doi:10.20944/preprints202011.0616.v1

dose Prop_H: 0.8 μM), disopyramide (Diso_L: 1.0, Diso_M: 2.0 and Diso_H: 5.0 μM) and quinidine (Quin_L: 1.0, Quin_M: 2.0 and Quin_H: 5.0 μM) [37, 87]. **Figure 5** shows the actions of disopyramide, quinidine and propafenone on $dVdt_{max}$ and APD_{90} in the AF condition. It can be seen in **Figure 5a** that disopyramide, quinidine and propafenone reduced $dVdt_{max}$ in a dose-dependent manner, with propafenone decreasing $dVdt_{max}$ to a greater extent than disopyramide and quinidine. Values of $dVdt_{max}$ upon application of disopyramide and quinidine were smaller than those in the drug-free AF condition, but were larger than that in the drug-free SR condition. However, values of $dVdt_{max}$ upon application of propafenone were smaller than those under drug-free AF and SR conditions. All drugs also prolonged APD_{90} in a dose-dependent manner (**Figure 5b**), with quinidine producing a slightly larger increase in APD_{90} across all concentrations investigated. In detail (**Table 6**), quinidine prolonged APD_{90} from 187.83 ± 25.56 ms in the drug-free AF condition to 217.89 ± 32.5 ms (Quin_L), 233.09 ± 38.73 ms (Quin_M) and 252.18 ± 42.67 ms (Quin_H), whereas values of APD_{90} are 191.29± 25.82 ms (Diso_L), 194.03± 25.99 ms (Diso_M) and 201.38± 26.54 ms (Diso_H) upon application of disopyramide, and are 202.55 ±28.40 ms (Prop_L), 210.71 ±30.96 ms (Prop_M) and 213.63 ±31.76 ms (Prop_H) upon application of propafenone. APD_{90} upon application of 5μM quinidine (Quin_H) in the AF condition is close to that in the drug-free SR condition (254.57 ± 41.51 vs. 252.18 ± 42.67).

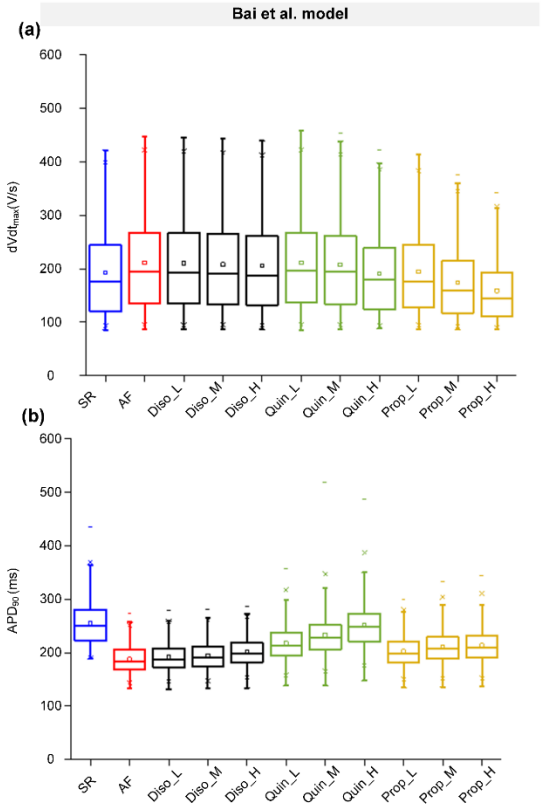

Figure 5. Effects of low (L), medium (M) and high (H) doses of disopyramide (Diso), quinidine (Quin) and propafenone (Prop) on the atrial fibrillation (AF) population using the Bai et al. model. (**a**) Simulated changes in the dVdtmax following the applications of drugs at different doses in comparison to the drug-free conditions in the AF population or in the normal population for sinus rhythm (SR). (**b**) Ranges of APD90 in conditions of drug-free SR, drug-free AF, AF in the presence of disopyramide at low (Diso_L), medium (Diso_M) and high (Diso_H) doses, AF in the presence of quinidine at low (Quin_L), medium (Quin_M) and high (Quin_H) doses, and AF in the presence of propafenone at low (Prop_L), medium (Prop_M) and high (Prop_H) doses.

Based on the experimentally-calibrated AF models created with the Grandi et al. model, antiarrhythmic effects of disopyramide, quinidine and propafenone on $dVdt_{max}$ and APD_{90} were investigated. **Figure 6** shows all drugs decreased $dVdt_{max}$ (**Figure 6a**) and prolonged APD_{90} (**Figure 6b**) in a dose-dependent manner. Consistent with results (**Figure 5**) obtained using the Bai et al. model,

Preprints (www.preprints.org) | NOT PEER-REVIEWED | Posted: 24 November 2020 doi:10.20944/preprints202011.0616.v1

propafenone decreased $dVdt_{max}$ to a greater extent than disopyramide and quinidine. Values of $dVdt_{max}$ upon application of propafenone and quinidine in the AF condition were smaller than that in the drug-free SR condition, but $dVdt_{max}$ upon application of disopyramide in the AF condition were larger than that in the drug-free SR condition (**Figure 6a**). It can also be seen in **Figure 6b** that APD_{90} upon application of disopyramide in the AF condition were larger than that in the drug-free SR condition, whereas values of APD_{90} upon application of propafenone and quinidine in the AF condition were smaller than that in the drug-free SR condition.

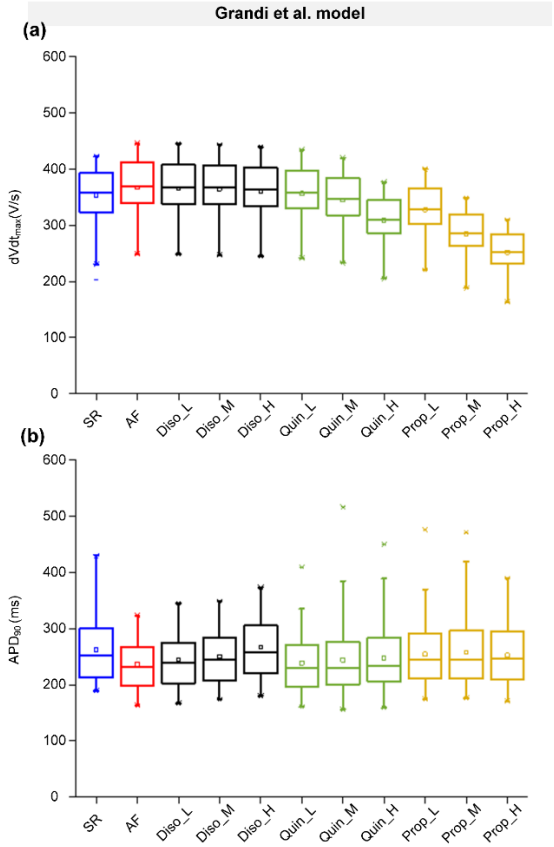

Figure 6. Effects of low (L), medium (M) and high (H) doses of disopyramide (Diso), quinidine (Quin) and propafenone (Prop) on the atrial fibrillation (AF) population using the Grandi et al. model. (**a**) Simulated changes in the $dVdt_{max}$ following the applications of drugs at different doses in comparison to the drug-free conditions in the AF population or in the normal population for sinus rhythm (SR). (**b**) Ranges of APD90 in conditions of drug-free SR, drug-free AF, AF in the presence of disopyramide at low (Diso_L), medium (Diso_M) and high (Diso_H) doses, AF in the presence of quinidine at low (Quin_L), medium (Quin_M) and high (Quin_H) doses, and AF in the presence of propafenone at low (Prop_L), medium (Prop_M) and high (Prop_H) doses.

Together, our models developed by the Bai et al. model or the Grandi et al. model predicted that all drugs reduced $dVdt_{max}$ and APD_{90} to a different extent. Among the three drugs, propafenone led to the most reduction in $dVdt_{max}$ and the least prolongation of APD_{90}. In addition, PPCs of ΔAPD_{90} and $\Delta dVdt_{max}$ for ionic properties (listed in **Table 1**) are shown in **Figure 3-4S** and **Figure 5-6S** in the Supplementary Material.

2.5 Antiarrhythmic effects of Class I drugs on CV and WL at the tissue level

To evaluate the effects of Class I drugs on *CV* and *WL*, we constructed one-dimensional (1D) models of human atrial strands with the Bai et al. model to investigate the responses of electrical waves to AADs in tissue. **Figure 7** shows *CV* and *WL* upon application of disopyramide, quinidine and propafenone in the AF condition, compared with those in the drug-free SR and AF conditions. *CV* was increased from 0.56 ± 0.09 mm/ms for the SR condition to 0.58 ± 0.09 mm/ms for the AF

Preprints (www.preprints.org) | NOT PEER-REVIEWED | Posted: 24 November 2020 doi:10.20944/preprints202011.0616.v1

condition. It can be seen in **Figure 7a** that disopyramide, quinidine and propafenone reduced *CV* in a dose-dependent manner, with quinidine and propafenone decreasing *CV* to a greater extent than disopyramide. Values of *CV* upon application of disopyramide and quinidine were smaller than those in the drug-free AF condition, but were larger than those in the drug-free SR condition. However, values of *CV* upon application of propafenone were smaller than those under drug-free AF and SR conditions (**Table 6**). **Figure 7b** shows values of *WL* under drug-free SR and AF conditions, and upon application of various concentrations of disopyramide, quinidine, and propafenone. *WL* was decreased from 141.05 ± 27.93 mm for the drug-free SR condition to 108.15 ± 20.19 mm for the drug-free AF condition. Compared with the drug-free AF condition, propafenone shortened *WL* in a dose-dependent manner, whereas disopyramide and quinidine prolonged *WL* in a dose-dependent manner. Quinidine prolonged *WL* to a greater extent than disopyramide. And upon application of 5μM quinidine (Quin_H) in the AF condition is close to that in the drug-free SR condition (132.22 ± 24.13 mm vs. 141.05 ±27.93 mm). In order of effects of AADs on WL, these drugs are quinidine, disopyramide and propafenone.

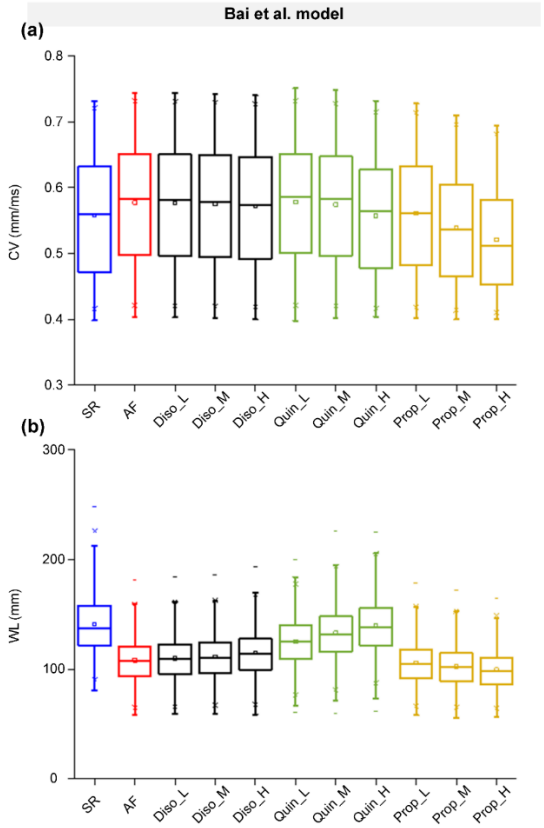

Figure 7. Effects of low (L), medium (M) and high (H) doses of disopyramide (Diso), quinidine (Quin) and propafenone (Prop) on the virtual tissue population for atrial fibrillation (AF) using the Bai et al. model. Simulated changes in conduction velocity (CV, **a**) and wavelength (WL, **b**) following the applications of drugs at different doses in comparison to the drug-free conditions in the AF population or in the normal population for sinus rhythm (SR).

Using 1D models of human atrial fibers developed with the Grandi et al. model, the antiarrhythmic effects of Class I drugs on *CV* and *WL* were also investigated. Consistent with results (**Figure 7a**) obtained using the Bai et al. model, all drugs decreased *CV* in a dose-dependent manner, with quinidine and propafenone decreasing *CV* to a greater extent than disopyramide (**Figure 8a**). In addition, values of *CV* upon application of various concentrations of propafenone were smaller than those under drug-free SR conditions. **Figure 8b** shows that disopyramide prolonged *WL* in a dose-dependent manner, whereas quinidine and propafenone shortened WL in a dose-dependent manner. However, values of WL upon application of quinidine (Quin_L and Quin_M) and propafenone

Preprints (www.preprints.org) | NOT PEER-REVIEWED | Posted: 24 November 2020 doi:10.20944/preprints202011.0616.v1

(Prop_L) were larger than those under the drug-free AF condition, indicating that quinidine is more effective that propafenone. In order of effects of AADs on *WL*, these drugs are disopyramide, quinidine and propafenone.

Quantitative summaries of the effects of Class AADs on human atrial electrical activity in the Pitx2-induced AF condition are listed in **Table 6** for the Bai et al. model and **Table 7** for the Grandi et al. model.

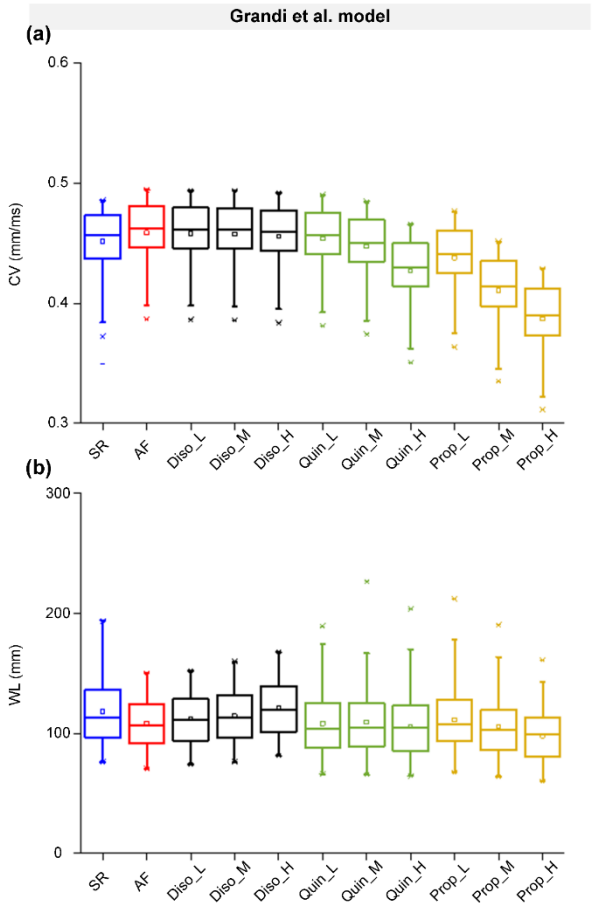

Figure 8. Effects of low (L), medium (M) and high (H) doses of disopyramide (Diso), quinidine (Quin) and propafenone (Prop) on the virtual tissue population for atrial fibrillation (AF) using the Grandi et al. model. Simulated changes in conduction velocity (CV, **a**) and wavelength (WL, **b**) following the applications of drugs at different doses in comparison to the drug-free conditions in the AF population or in the normal population for sinus rhythm (SR).

Table 6. A quantitative summary of the effects of Class I antiarrhythmic drugs on human atrial electrical activity using the Bai et al. model.

Model		*Cell*		*Tissue*	
		dVdtmax(V/s)	*APD90 (ms)*	*CV (m/s)*	*WL (mm)*
SR		192.82 ±81.23	254.57 ±41.51	0.56 ±0.09	141.05 ±27.93
AF		210.72 ±86.83	187.83± 25.56	0.58 ±0.09	108.15 ±20.19
Disopyramide	*Diso_L*	209.74 ± 86.35	191.29 ± 25.82	0.58 ± 0.09	109.83 ± 20.28
	Diso_M	208.31 ± 87.00	194.03 ± 25.99	0.57 ± 0.09	111.12 ± 20.51
	Diso_H	205.54 ± 84.96	201.38 ± 26.54	0.57 ± 0.09	114.69 ± 21.23
Quinidine	*Quin_L*	211.47 ± 86.32	217.89 ± 32.5	0.58 ± 0.09	125.25 ± 22.55
	Quin_M	207.26 ± 84.45	233.09 ± 38.73	0.57 ± 0.09	132.22 ± 24.13
	Quin_H	190.69 ± 76.09	252.18 ± 42.67	0.56 ± 0.09	139.39 ± 25.64
Propafenone	*Prop_L*	194.09 ± 77.34	189.07 ± 25.38	0.56 ± 0.09	105.74 ± 19.54
	Prop_M	174.28 ± 66.56	190.41 ± 25.45	0.54 ± 0.08	102.22 ± 18.92
	Prop_H	158.88 ± 58.10	191.55 ± 25.38	0.52 ± 0.08	99.49 ± 18.16

Preprints (www.preprints.org) | NOT PEER-REVIEWED | Posted: 24 November 2020 doi:10.20944/preprints202011.0616.v1

Table 7. A quantitative summary of the effects of Class I antiarrhythmic drugs on human atrial electrical activity using the Grandi et al. model.

Model		*Cell*		*Tissue*	
		dVdtmax(V/s)	*APD90 (ms)*	*CV (m/s)*	*WL (mm)*
SR		353.19 ± 50.01	261.84 ± 58.49	0.45 ± 0.03	118.18 ± 27.28
AF		367.42 ± 48.68	236.52 ± 42.76	0.46 ± 0.03	108.46 ± 19.82
	Diso_L	365.48 ± 48.12	244.62 ± 44.82	0.46 ± 0.03	111.97 ± 20.82
Disopyramide	***Diso_M***	364.40 ± 47.98	250.31 ± 45.44	0.46 ± 0.03	114.45 ± 21.17
	Diso_H	360.88 ± 47.65	266.77 ± 50.21	0.46 ± 0.03	121.50 ± 23.26
	Quin_L	356.78 ± 47.21	238.34 ± 52.20	0.45 ± 0.03	108.11 ± 24.16
Quinidine	***Quin_M***	344.65 ± 45.97	244.11 ± 65.35	0.45 ± 0.03	109.17 ± 29.45
	Quin_H	309.11 ± 42.09	247.18 ± 57.03	0.43 ± 0.03	105.66 ± 26.01
	Prop_L	327.77 ± 43.93	254.35 ± 57.65	0.44 ± 0.03	111.28 ± 25.47
Propafenone	***Prop_M***	284.55 ± 39.37	257.36 ± 59.32	0.41 ± 0.03	105.70 ± 25.03
	Prop_H	251.47 ± 35.88	252.69 ± 51.50	0.39 ± 0.03	97.86 ± 21.21

Collectedly, alterations in *WL* predicted with the Bai et al. model were different from those predicted with the Grandi et al. model, but simulated results indicated that disopyramide and quinidine are more effective than propafenone. In addition, PPCs of Δ *CV*and Δ *WL* for ionic properties (listed in **Table 1**) are shown in **Figure 7-8S** and **Figure 9-10S** in the Supplementary Material.

3. Discussion

Population-based studies have assessed the influence of common single-nucleotide polymorphisms related to AF on the response to AAD therapies and showed that carriers of the variant allele at rs10033646 on chromosome 4q25 responded favorably to the Class I AADs [34]. The actions of Class I AADs disopyramide, quinidine, and propafenone were assessed in the context of Pitx2-induced AF using a population-based Quantitative Systems Pharmacology Framework [55]. Through sensitivity and statistical analyses of our atrial cell and tissue populations, we found that *WL* prolongation could be achieved by quinidine and disopyramide. This study provides clinically-relevant insights into the pharmacology of *WL* prolongation by evaluating and comparing the actions of all three drugs in the context of Pitx2-induced AF, offering an important step toward in silico optimization of pharmacological therapy in this context.

3.1 Main findings

The major findings presented in this study are as follows. (1) Populations of models based on two human atrial AP models are able to mimic a wide range of inter-subject variability in human atrial AP properties as exhibited in a set of AP measurements from over 379 SR and AF patients. (2) Pitx2-induced remodelling (as reported in [36]) predicts abbreviated APD_{90} and increased $dVdt_{max}$ at the cellular level, and increased *CV* and shortened *WL* at the tissue level in SR versus AF conditions, as reported in experimental studies [17, 59] (**Table 2**). (3) AP biomarkers (namely APD_{90} and $dVdt_{max}$) are correlated in both SR and AF cardiomyocytes created with the Bai et al. and the Grandi et al. models. $dVdt_{max}$ is primarily determined by G_{Na}, whereas APD_{90} is determined by G_{CaL}, G_{Ks} and G_{K1}. (4) AADs disopyramide, quinidine, and propafenone prolonged APD_{90} and decreased $dVdt_{max}$ and *CV* in a dose-dependent manner in drug-free versus drug-bound AF conditions. (5) Disopyramide and quinidine prolonged *WL*, whereas propafenone shortened *WL*. Disopyramide and quinidine are more effective against Pitx2-induced AF than propafenone. A summary of findings regarding pro-arrhythmic mechanisms of Pitx2-induced AF and anti-arrhythmic actions of selected Class I drugs is given in **Figure 9.**

Preprints (www.preprints.org) | NOT PEER-REVIEWED | Posted: 24 November 2020 doi:10.20944/preprints202011.0616.v1

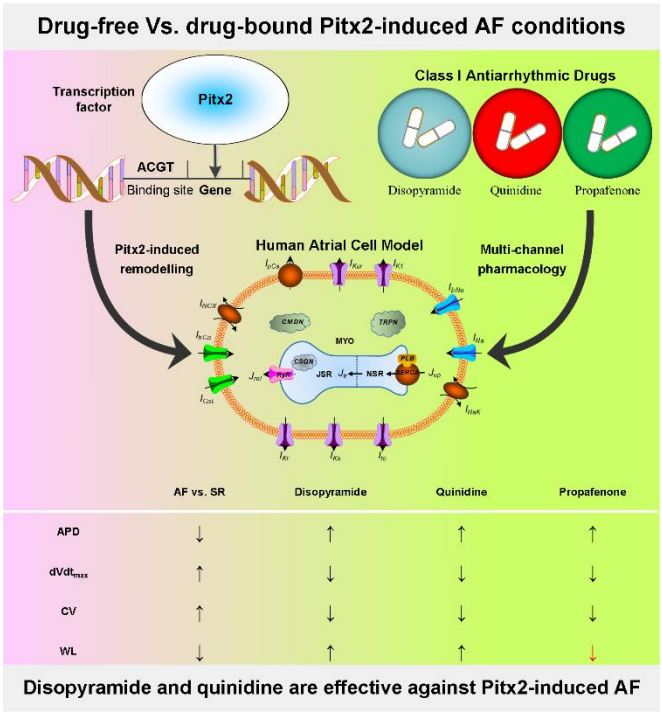

Figure 9. A summary of findings regarding pro-arrhythmic mechanisms of Pitx2-induced AF and anti-arrhythmic actions of selected Class I drugs disopyramide, quinidine and propafenone on APD, $dVdt_{max}$, CV and WL.

3.2 Changes in AP are linked to Pitx2-induced remodelling

Research studies on Pitx2-induced AF have demonstrated that Pitx2-induced remodelling contributes to atrial cellular electrophysiological changes in AF patients [11, 17, 26]. Experimental data showed that alterations in human atrial AP included AP shortening and increased upstroke velocity [59] and our simulated effects of Pitx2-induced remodelling on AP (**Table 2** and **Table 5**) are concordant with these experimental findings.

Previous experiments on isolated human atrial myocytes have demonstrated that Pitx2-induced remodelling of ion channels, particularly for I_{Ks} and I_{CaL}, may contribute to the clinically significant association between impaired Pitx2 and AF [26]. Further simulations in our previous study indicated the Pitx2-induced changes in I_{Ks} and I_{CaL} led to APD shortening, facilitating sustained re-entry in 3D anatomical atrial geometry [30]. Our simulations in the Pitx2-induced AF population of models show that AP shortening is determined by I_{CaL} and I_{Ks}, and APD is negatively correlated with I_{Ks} and positively correlated with I_{CaL} (**Figure 4**). This is consistent with findings from previous studies that upregulation of I_{Ks} and downregulation of I_{CaL} due to Pitx2-induced remodelling critically contribute to the abbreviation of APD [30, 33].

Furthermore, increased upstroke velocity in Pitx2-induced AF may be resulted from remodelled I_{Na} arising from impaired Pitx2. Previous experiments in atrial cardiomyocytes of Pitx2-deleted mice showed increased action potential amplitude and shortened APD [17]. Further gene analysis showed that reduced Pitx2 dose caused an increase in the expression of SCN5A [17] encoding the alpha subunit of the human cardiac voltage-gated sodium channel (I_{Na}). In addition, an increase in the mRNA level of SCN1B encoding a beta-1 subunit of voltage-gated sodium channels (I_{Na}) was observed in patients with familial AF arising from the Pitx2c mutation p.Met207Val [61]. Decreased mRNA levels of SCN5A and SCN1B were also observed in atrial-specific Pitx2 mutant mice [22, 25], but changes in T-box transcription factor Tbx5 was not investigated and downregulation of sodium channel genes may be resulted from impaired Tbx5. Previous experiments in atrial cardiomyocytes of Tbx5-deleted mice showed reduced Pitx2 and sodium channel genes although reduced Pitx2 without alterations in Tbx5 caused an increase in sodium channel genes [17]. Based on these data on remodelled I_{Na} due to impaired Pitx2, Pitx2-induced AF model was developed and predicted an

 doi:10.20944/preprints202011.0616.v1

increase in action potential amplitude and maximum upstroke velocity [36]. Consistent with these findings, our simulations in the Pitx2-induced AF population of models show that increased upstroke velocity is determined by I_{Na} and is positively correlated with I_{Na} (**Figure 4**). Further simulations at the tissue level predicted that increased I_{Na} led to fast conduction of AP propagation.

3.3 Anti-arrhythmic effects of Class I drugs in Pitx2-induced AF

Despite the prevalence of AF and decades of research, antiarrhythmic therapies for AF continue to have limited efficacy and safety [35]. A population-based study assessed the influence of AF-associated loci on the response to antiarrhythmic drug therapies and showed that carriers of the variant allele at rs10033646 on chromosome 4q25 (Pitx2) responded favorably to Class I AADs [34]. And Class I AADs frequently used clinically include flecainide, disopyramide, quinidine and propafenone [35]. Anti-arrhythmic effects of flecainide on Pitx2-induced AF were investigated in our previous study and simulation results indicated that flecainide has antiarrhythmic effects on AF due to impaired Pitx2 by preventing spontaneous calcium release and increasing wavelength [36]. In the present study, the effectiveness of disopyramide, quinidine and propafenone was assessed with *WL*. Simulated results showed that disopyramide and quinidine were moderately effective by prolonging *WL*, whereas propafenone was shown to be ineffective by abbreviating *WL* in Pitx2-induced AF (**Table 6**). *WL* is the product of APD_{90} and *CV*. Increased APD_{90} (**Figure 5**) and decreased *CV* (**Figure 7**) occurred upon the application of disopyramide, quinidine and propafenone. Under the application of disopyramide or quinidine, the extent of AP prolongation is larger than the degree of *CV* reduction, resulting in an increase in *WL*. In contrast, the extent of *CV* reduction is much larger than the degree of AP prolongation, leading to a reduction in *WL*. Alterations in *WL* can be linked to block effects of Class I drugs on ion channels (**Table 4**) which included G_{Na}, G_{CaL}, G_{to}, G_{Ks}, G_{Kr}, G_{Kur} and G_{K1}. Under the application of Class I drugs in Pitx2-induced AF, inhibition of sodium currents would decrease $dVdt_{max}$ and thereby reduce CV, while block of potassium currents would prolong APD_{90}. Therefore, the antiarrhythmic effects of Class I drugs in Pitx2-induced AF can be attributed to their potent block of sodium and potassium channels. And the effectiveness of drugs is determined by the extent of their block effects on sodium and potassium channels. Therefore, disopyramide and quinidine are more effective than propafenone in Pitx2-induced AF and this is because the extent of their block effects on potassium channels is larger than that on sodium channels. Collectively, our results demonstrate that a combined block of sodium and potassium currents can exert synergistic antiarrhythmic effects and therefore is a valuable therapeutic for Pitx2-induced AF.

3.4 Model- and AP-shape independence of prediction of the antiarrhythmic effects of Class I drugs

It is well known that human atrial myocytes display two distinct AP morphologies: the type-1 AP shows a notch-and-dome morphology and the type-3 AP shows a typical triangular morphology [59, 62]. Therefore, Bai et al. model displaying the type-1 AP [27] and Grandi et al. model displaying the type-3 AP [60] were chosen to generate populations of human atrial AP. According to the stimulation protocol (1Hz) used in experiments [59], we ran simulations and reproduced Pitx2-induced AP morphology, with both $dVdt_{max}$ increase and AP shortening being reported experimentally [59]. Further simulations predicted the antiarrhythmic effects of Class I drugs on APD_{90} and $dVdt_{max}$, but their effects are dependent on baseline AP morphology [88, 89] seen in previous modelling [55]. While some of the differences in model responses might be related to distinct AP morphologies, we cannot exclude model-dependencies due to distinct cellular model structure and models of ionic and calcium handling processes. Interestingly, analyses using both models demonstrated that these Class I drugs disopyramide, quinidine and propafenone prolonged APD_{90} and reduced $dVdt_{max}$ in a dose-dependent manner. Therefore, these results demonstrated that these Class I drugs consistently produced anti-AF effects independent of the baseline electrophysiological characteristics.

Although Class I drugs disopyramide, quinidine and propafenone produced similar anti-AF effects (AP prolongation and $dVdt_{max}$ and *CV* reduction), the degree of changes in APD_{90} and $dVdt_{max}$ is different between Bai et al. model and Grandi et al. model. According to the extents of $dVdt_{max}$ and

CV reduction, drugs with both Bai et al. and Grandi et al. models are sorted as propafenone> quinidine>disopyramide. However, based on the degrees of AP prolongation, drug ranking obtained with the Bai et al. model is quinidine> disopyramide> propafenone, whereas drugs whose effects were predicted with the Grandi et al. model are ranked as disopyramide> quinidine> propafenone. Different alterations in *CV* and APD_{90} leading to different changes in *WL*, which can be used as one of the indexes for evaluating the antiarrhythmic effects of drugs at the tissue level [55]. If the extent of AP prolongation is larger than that of *CV* reduction, *WL* is prolonged. Conversely, *WL* is shortened. For the Bai et al., model, *WL* is prolonged upon application of quinidine and disopyramide, but is shortened upon application of propafenone. However, for the Grandi et al. model, *WL* upon application of disopyramide at various concentrations, quinidine at low and medium concentrations and propafenone at the low concentration is prolonged, but is shortened upon application of quinidine at the high concentration and propafenone at medium and high concentrations. Based on alterations in *WL*, drug ranking obtained with the Bai et al. model is quinidine> disopyramide> propafenone, whereas drugs are sorted as disopyramide>quinidine> propafenone for the Grandi et al. model. Therefore, analyses using both models demonstrated that quinidine and disopyramide are more effective against Pitx2-induced AF than propafenone.

3.5 Limitations and Future Work

Several limitations specific to this study are addressed here. Firstly, the electrophysiological representation of AF-induced remodelling in the human atrial AP model is based on data from previous mice models of Pitx2-induced AF, however, because of the lack of experimental data on humans. Special attention must be paid to the differences between mice and human atrial cells [90]. Further, we simulated AF model populations with all identified targets associated with impaired Pitx2 [11, 17, 18, 22, 23, 26]. However, Pitx2-induced remodelling is different in published experimental studies [11, 17, 18, 22, 23, 26], atrial cell types [11], AF stages [91] and AF patients with different age [92]. The complexity of Pitx2-induced remodelling may present complex responses to these Class I drugs and require more realistic heterogenous descriptions in cellular and tissue simulations. Secondly, effects of these Class I AADs on ion currents were modelled by changing maximum current conductances with a simple pore block scheme based on IC_{50} and *nH* values, but it might be important to incorporate state-dependence and use-dependence of antiarrhythmic drugs in evaluating realistic compounds [37, 63, 87]. Model variations for these characteristics (including the affinity of the drug compound to various gating modalities, binding kinetics, drug polarity, charge for the drug-channel interaction and so on) are far beyond the scope of the current study and should be explored in future studies. In addition, IC_{50} values are chosen based on experimental data from atrial cells (where data are available) and large ventricular cells (where atrial data are not available), but the large variability in IC_{50} was influenced by various experimental conditions, including different species, different cell types [93], temperature [94], ionic concentrations and voltage-clamp protocols. Therefore, special attention should be paid to explain our simulated results. Thirdly, considering the stimulation protocol used under the experimental conditions [59], we performed all simulations only at 1Hz and rate-dependent APD modulation will be further investigated when experimental data at different frequencies are available. Here, we only used APD_{50}, APD_{90}, *RMP* and $dVdt_{max}$ as biomarkers to calibrate populations of human atrial AP models. And parameter unidentifiability, which can be attenuated if broader experimental datasets are available, is a potential limitation. Finally, we analyzed the effects of Class I drugs by quantifying changes in APD_{90} and $dVdt_{max}$ at the cellular level and *CV* and *WL* in tissue. This approach is consistent with the accepted mechanisms of action of Class I drugs and is limited in that it didn't account for composite metrics, including calcium-associated biomarkers, afterdepolarizations, alternans and AP propagation dynamics. Nevertheless, mechanisms underlying actions of Class I drugs are highly complex and future investigations should be carried out.

Preprints (www.preprints.org) | NOT PEER-REVIEWED | Posted: 24 November 2020 doi:10.20944/preprints202011.0616.v1

4. Materials and Methods

4.1. Experimantal dataset

The Experimental dataset on AP recordings was used in the present study for calibration of the human atrial electrophysiology. The data set published in the previous study [59] comprised of 480 instances from 379 patients: AP recordings from n=256 right atrial appendages of N = 221 SR patients and from n=224 right atrial appendages of N = 158 AF patients. Human myocytes were isolated enzymatically from atrial appendages and APs were recorded with standard intracellular microelectrodes in atrial trabeculae. Preparations were electrically stimulated at a single constant rate of 1 Hz for 60 min with isolated square-wave stimuli of 1 ms duration, two times threshold intensity. Obtained human atrial APs displayed spike-and-dome and a more triangular conformation. The following parameters were quantified to characterize intersubject variability in human atrial AP: $dVdt_{max}$, *RMP*, and APD_{50} and APD_{90}. Compared with APs of SR myocytes, APD_{50} and APD_{90} were reduced and $dVdt_{max}$ was increased for APs of AF atrial cells (**Table 2**). More information (including ethics approval, informed consent and basic information of participants) regarding the experimental conditions under which the data were collected is available in the study of Ravens et al [59].

4.2. Mathematical models representing distinct morphological subtypes of human atrial AP

To represent spike-and-dome and a triangular conformation of human atrial APs observed in experiments [59, 62], the Bai et al. model displaying a type-1 AP with notch-and-dome morphology and the Grandi et al. model displaying a type-3 AP with typical triangular shape were chosen as a base to construct the computational AP model populations.

The Bai et al. model developed by our group is able to reproduce human AP morphology, APD rate dependence and triggered activity, i.e., early afterdepolarizations (EADs), delayed afterdepolarizations (DADs) and spontaneous depolarizations [27]. This biophysically-detailed model of human atrial cellular electrophysiology also has been used to investigate mechanisms underlying Pitx2-induced AF and here we provide a brief description. It includes representation of the 13 transmembrane ionic currents and 2 main intracellular calcium flows, including fast sodium current (I_{Na}), transient outward potassium current (I_{to}), rapid delayed rectifier potassium current (I_{Kr}), slow delayed rectifier potassium current (I_{Ks}), ultrarapid delayed rectifier potassium current (I_{Kur}), inward rectifier potassium current (I_{K1}), L-type calcium current (I_{CaL}), background sodium current (I_{BNa}), background calcium current (I_{BCa}), plateau potassium current (I_{PK}), plateau calcium current (I_{PCa}), sodium-potassium pump current (I_{NaK}), sodium-calcium exchange current (I_{NCX}), the calcium flow (I_{up}) through the sarcoplasmic reticulum calcium ATPase (SERCA) and calcium release flow (I_{rel}).

Comparative simulations were carried out using the human atrial cell model of Grandi et al. [60, 95] (GB model). The baseline GB model was modified to generate the Grandi et al. model to facilitate AP propagation in tissue by replacing I_{Na} formulation with that of the human cell model [96, 97]. The Grandi et al. model includes representation of the 18 transmembrane ionic currents and 2 main intracellular calcium flows, including I_{to}, I_{Kr}, I_{Ks}, I_{Kur}, I_{K1}, I_{CaL}, I_{BNa}, I_{BCa}, I_{PK}, I_{PCa}, I_{NaK}, I_{Ncx}, I_{up}, I_{rel}, sodium current through the L-type calcium channel (I_{CaNa}), potassium current through the L-type calcium channel (I_{CaK}), calcium-activated chloride current (I_{ClCa}), background chloride current (I_{BCl}), late sodium current (I_{NaL}) and I_{Na}. This I_{Na} model [96, 97] is given by

$$I_{Na} = G_{Na} m^3 hj (V_m - E_{Na}) \tag{1}$$

$$m_\infty = 1.0/[1.0 + e^{\langle -56.86 - V_m \rangle / 9.03}]^2 \tag{2}$$

$$\tau_m = \{1.0/[1.0 + e^{\langle -60 - V_m \rangle / 5}]\}\{0.1/[1.0 + e^{\langle V_m + 35 \rangle / 5}] + 0.1/[1.0 + e^{\langle V_m - 50 \rangle / 200}]\} \tag{3}$$

$$h_\infty = 1.0/[1.0 + e^{\langle 71.55 + V_m \rangle / 7.43}]^2 \tag{4}$$

$$\alpha_h = 0 \ (V_m \geq -40) \tag{5}$$

Preprints (www.preprints.org) | NOT PEER-REVIEWED | Posted: 24 November 2020 doi:10.20944/preprints202011.0616.v1

$$\alpha_h = 0.057e^{-\langle V_m+80\rangle/6.8}\ (V_m < -40)$$

$$\beta_h = 0.77/[0.13(1.0 + e^{-\langle V_m+10.66\rangle/11.1})]\ (V_m \geq -40)$$
$$\beta_h = 2.7e^{0.079V_m} + 310000e^{0.3485V_m}(V_m < -40) \quad (6)$$

$$\tau_h = 1.0/(\alpha_h + \beta_h) \quad (7)$$

$$j_\infty = 1.0/[1.0 + e^{\langle 71.55+V_m\rangle/7.43}]^2 \quad (8)$$

$$\alpha_j = 0\ (V_m \geq -40)$$
$$\alpha_j = \langle -25428e^{0.2444V_m} + 0.000006948e^{-0.04391V_m}\rangle(V_m + 37.78)/(1.0 + e^{0.311\langle 79.23+V_m\rangle})\ (V_m < -40) \quad (9)$$

$$\beta_j = 0.6e^{0.057V_m}/(1.0 + e^{-0.1\langle 32+V_m\rangle})\ (V_m \geq -40)$$
$$\beta_j = 0.02424e^{-0.01052V_m}/(1.0 + e^{-0.1378\langle 40.14+V_m\rangle})(V_m < -40) \quad (10)$$

$$\tau_j = 1.0/(\alpha_j + \beta_j) \quad (11)$$

where G_{Na}(14.838 nS/pF) is the maximal conductance, m, h and j are three gate variables for I_{Na}. V_m is the membrane potential, and E_{Na} is the sodium equilibrium potential. m_∞, h_∞ and j_∞ denote steady-state activation, steady-state inactivation and steady-state inactivation, respectively. τ_m, τ_h and τ_j are the time constants for m_∞, h_∞ and j_∞, respectively.

Based on these models of ion channels, the electrophysiological behavior of human atrial cells can be modelled with the following differential equation:

$$dV_m/dt = -(I_{ion} + I_{stim})/C_m \quad (12)$$

where V_m is the membrane potential, t is time, I_{ion} is the total sum of transmembrane ionic currents (listed in **Table 1**), I_{stim} is the externally applied stimulus current with amplitude of -80 $\mu A/\mu F$ and a duration of 0.5 ms, and C_m is the membrane capacitance (1 μF).

In order to investigate the electrophysiological behavior of human atrial tissues, a multicellular model of homogeneous atrial tissue with 200 nodes spaced evenly by 0.15 mm was constructed to quantify APD_{90} and CV for calculating WL. The propagation of APs was governed by the partial differential equation:

$$dV_m/dt = -(I_{ion} + I_{stim})/C_m + D(\partial^2 V_m/\partial x^2) \quad (13)$$

where D is a scalar coefficient describing the intercellular electrical coupling via gap junctions. In simulations, D was set to be a constant value of 0.154 mm^2ms^{-1} that gave a CV of 0.65 m/s for the Bai et al. model and 0.59 m/s for the Grandi et al. model. The resulting CVs were comparable to those seen in atrial tissue [98, 99]. Time (t) step was 0.02 ms for the Bai et al. model and 0.005 ms for the Grandi et al. model, respectively.

4.3. Modelling Pitx2-induced AF

To obtain human AF myocytes models that reproduced the experimentally observed changes in the mRNA levels corresponding to key proteins under Pitx2-induced electrical remodelling conditions, we assumed that these changes in mRNA expression are quantitatively reflected at the final functional level of ion channels [29] and incorporated alterations in the maximal conductances of ionic currents due to Pitx2-induced electrical remodelling into the Bai et al. (or the Grandi et al.) model. These Pitx2-induced changes in the ionic channel properties have been well characterized in many experimental studies [17, 18, 23-26, 61]. However, the identified targets were different among these studies: while several studies showed no Pitx2-associated changes [18] and reductions [22, 25] in sodium channel gene expression, significant increases [17, 61] in this channel gene expression have also been well-documented. Similarly, calcium channel gene expression was found decreased in this

 doi:10.20944/preprints202011.0616.v1

study[12], but increased in others [22, 23, 25, 26]. Further, whereas overexpression of potassium gene encoding I_{K1} was identified in the study of Kirchhof et al.[11], underexpression of this gene was observed in some studies [18, 22]. In addition, all these studies have shown upregulation of genes encoding I_{Ks} [11, 12, 15, 26, 61], I_{rel} [12, 17, 23, 25]and I_{up}[22, 24, 67, 70, 71]. Modifications made for each model are summarized in **Table 3**.

4.4. Simulations of actions of Calss I AADs in Pitx2-induced AF

In our previous studies [37, 87], the actions of Class I AADs disopyramide, quinidine and propafenone on human atrial electrophysiology were simulated in the setting of hERG-linked short QT syndrome[37]. The effects of these Class I AADs on ion currents were modelled by changing maximum current conductances with a simple pore block scheme based on IC_{50} and nH [31]. Maximum current conductances associated with these drugs included G_{Na}, G_{CaL}, G_{to}, G_{Ks}, G_{Kr}, G_{Kur} and G_{K1}. For disopyramide, as measured in previous studies, values of IC_{50} for G_{Na}, G_{CaL}, G_{to}, G_{Ks}, G_{Kr} and G_{Kur}, respectively, were taken to be 168.4 μM [65], 1036.7 μM [65], 20.9 μM [69], 88.1 μM [72], 14.4 μM [65] and 25.0μM [75]. For quinidine, as observed in experimental studies, G_{Na}, G_{CaL}, G_{to}, G_{Ks}, G_{Kr}, G_{Kur} and G_{K1} were decreased with an IC_{50} of 14.6μM [65], 14.9μM [67], 21.8μM [70], 44.0μM [73], 0.72μM [65], 6.6μM [70] and 42.6μM [70], respectively. Propafenone decreased G_{Na}, G_{CaL}, G_{to}, G_{Kr}, G_{Kur} and G_{K1} with an IC_{50} of 1.2μM [66], 1.7μM [68], 4.8μM [71], 2.0μM [74], 4.4μM [76] and 16.8μM [77], respectively. Taking into account plasma protein binging, estimates of the most likely unbound concentrations of disopyramide, quinidine and propafenone have been given as 1-15 μM [86, 100], 1-15 μM [86, 100] and 0.15-1 μM[83-85]. The effects of low (L), medium (M) and high (H) doses within the therapeutic ranges of disopyramide (Diso_L: 1.0, Diso_M: 2.0 and Diso_H: 5.0 μM), quinidine (Quin_L: 1.0, Quin_M: 2.0 and Quin_H: 5.0 μM)) and propafenone ((Prop_L: 0.2, Prop_M: 0.5 and Prop_H: 0.8 μM)) were studies.

4.5. Generation and calibration of populations of models

To capture intersubject variability, populations of sampled models of human atrial electrophysiology for SR were generated based on the Bai et al. and the Grandi et al. models. All models in each population shared the same equations but parameters of ionic current conductances in determining the human atrial AP were varied with respect to their original values. These parameters were independently varied following a log-normal distribution and sigma was set to be 0.2 to cover a range of variability similar to that seen in experiments based on previous studies [41, 55, 63, 64]. The size of the SR population was set to be 1200 for convergence of the sensitivity coefficients [101]. Following the ASME V&V40 Standard proposed by the Subcommittee of the American Society of Mechanical Engineers (ASME) on Verification and Validation (V&V) in Computational Modeling of Medical Devices [102] for developing a structured approach for establishing the credibility of computational models for a specific use, we used the candidate models to simulate human atrial AP by considering stimulation frequency (1Hz) under the experimental conditions [59] and calculate AP biomarkers of each candidate model. The candidate models generated in the previous step were selected to constitute the SR population whose simulated electrophysiological properties are within 3 standard error from the mean experimental values in SR patient data on AP biomarkers (including $dVdt_{max}$, RMP, APD_{50} and APD_{90}) in **Table 2**. This step yields the experimentally-calibrated population of models. Modifications to ionic currents due to Pitx2-induced remodelling (**Table 3**) were introduced into SR model variants to generate the candidate AF models. These candidate AF models were calibrated to 3 standard error from the mean experimental values in AF patient data (**Table 2**). Then, actions of Class I AADs on ion channels were incorporated into the experimentally-calibrated AF models to investigate their effects on $dVdt_{max}$, APD_{90}, CV and WL.

Preprints (www.preprints.org) | NOT PEER-REVIEWED | Posted: 24 November 2020 doi:10.20944/preprints202011.0616.v1

4.6. Simulation protocols

The stimulation protocol mimics the one used by Ravens et al.[59] to obtain AP measurements in SR and AF cardiomyocytes. Cell mathematical models were initially preconditioned by pacing at a basic cycle length of 1000 ms until the steady-state was reached. A stimulus with an amplitude of $-80\ \mu A/\mu F$ and a duration of 0.5 ms is applied at each pace.

Considering computational cost for reaching steady-state, a series of 10 conditioning waves was initiated by supra-threshold stimuli with an amplitude of $-80\ \mu A/\mu F$ and a duration of 1.0 ms to the 3 nodes at the strand end. The last beat was recorded for APD_{90} and CV analysis.

4.7. Sensitivity analysis

To quantify the relative importance of ionic conductances in determining changes in AP biomarkers, PCCs were used on the SR and AF populations to evaluate the role of each ionic current [101]. Partial correlation is a method to find correlations between two variables, after accounting for the linear effects of one or more additional variables [103]. PCC between x and y, given the set of N additional variables z_i, is then defined as the correlation coefficient between the residuals $r_x = x - \hat{x}$ and $r_y = y - \hat{y}$ [101]. $\hat{x}$ and $\hat{y}$ are the respective sample means or the following linear regression models:

$$\hat{x} = c_0 + \sum_{i=1}^{N} c_i z_i \qquad and \qquad \hat{y} = b_0 + \sum_{i=1}^{N} b_i z_i \tag{14}$$

$$PPC(x, y, z_i) = \frac{Cov(r_x, r_y)}{Var(r_x)Var(r_y)} \tag{15}$$

where $Cov(r_x, r_y)$ represents the covariance between r_x and r_y, while $Var(r_x)$ and $Var(r_y)$ are respectively the variance of r_x and variance of r_y.

4.7. Software, numerical methods and statistical analysis

The Bai et al. (available from the repository CellML http://models.cellml.org/workspace/520)and the Grandi et al. models (freely available at https://github.com/drgrandilab) was implemented in MATLAB 2018a (The MathWorks, Natick, MA, USA) using the stiff ordinary differential equation solver ode15s and analysis of biomarkers was also performed using MATLAB. In addition, the 1D models were implemented in C++. The ODEs were solved using the Forward Euler method. Our user project containing newly created datasets and the simulation codes used in this study is available to download from the GitHub website (https://github.com/aspirerabbit). All simulations and data analyses were performed on a computing cluster with Intel(R) Xeon(R) CPU E5-2690 v4 @ 2.60GHz 32 CPUs 28 CPUs (56 threads) + 128GB. Statistical significance in differences on ionic conductance distributions between populations was evaluated by using the Mann-Whitney U test. A probability <0.05 was considered statistically significant.

5. Conclusions

In conclusion, populations of models reproduce the variability in human atrial AP properties measured in samples obtained from patients and AF models predict AP shortening and fast conduction in Pitx2-induced remodelling conditions observed in experiments. State-of-the-art Quantitative Systems Pharmacological simulations demonstrated that disopyramide, quinidine and propafenone produce AP prolongation and slow conduction in the setting of Pitx2-induced AF. However, disopyramide and quinidine were more effective in prolonging WL than propafenone.

Supplementary Materials: Supplementary materials can be found at www.mdpi.com/xxx/s1.

Author Contributions: Conceptualization, Y.Z., J.B., M.G., J.Z. and H.Z.; methodology, M.G. and Y.Z.; software, Y.Z.; validation, Y.Z., M.G. and J.B.; formal analysis, Y.Z. , M.G. and J.B.; investigation, Y.Z., M.G. and J.B.; resources, Y.Z. and J.B.; data curation, Y.Z. , M.G. and J.B.; writing—original draft preparation, M.G. and J.B.;

writing—review and editing, Y.Z., J.B., M.G., A.L., Y.L., J.Z. and H.Z.; visualization, Y.Z., M.G. and J.B.; supervision, J.B. and Y.L.; project administration, J.B. and Y.L.; funding acquisition, J.B. and Y.L. All authors have read and agreed to the published version of the manuscript.

Funding: This research was funded by the National Natural Science Foundation of China, grant number 61901192 (J.B.) National Key Research and Development Project, grant number 2019YFC0120100 and 2019YFC0121907 (J.B. and Y.L.).

Acknowledgments: We would like to thank Minghong Zhou and Chuan Wang for technical support.

Conflicts of Interest: The authors declare no conflict of interest.

Abbreviations

AF	atrial fibrillation
GWAS	genome-wide association studies
Pitx2	paired-like homeodomain transcription factor 2
AAD	antiarrhythmic drug
AP	action potential
APD	AP duration
$dVdt_{max}$	maximum upstroke velocity
CV	conduction velocity
WL	wavelength
SR	sinus rhythm
RMP	resting membrane potential
APD_{50}	AP duration at 50%
APD_{90}	AP duration at 90%
IC_{50}	half-maximal inhibitory concentration
nH	Hill-coefficient value
PCC	partial correlation coefficient
Prop_L	low dose of propafenone
Prop_M	medium dose of propafenone
Prop_H	high dose of propafenone
Diso_L	low dose of disopyramide
Diso_M	medium dose of disopyramide
Diso_H	high dose of disopyramide
Quin_L	low dose of quinidine
Quin_M	medium dose of quinidine
Quin_H	high dose of quinidine
1D	one-dimensional
I_{Na}	fast sodium current
I_{to}	transient outward potassium current
I_{Kr}	rapid delayed rectifier potassium current
I_{Ks}	slow delayed rectifier potassium current
I_{Kur}	ultrarapid delayed rectifier potassium current
I_{K1}	inward rectifier potassium current
I_{CaL}	L-type calcium current
I_{BNa}	background sodium current
I_{BCa}	background calcium current
I_{PK}	plateau potassium current
I_{PCa}	plateau calcium current
I_{NaK}	sodium-potassium pump current
I_{Ncx}	sodium-calcium exchange current
I_{up}	the calcium flow through the sarcoplasmic reticulum calcium ATPase (SERCA)
I_{rel}	calcium release flow
I_{CaNa}	sodium current through the L-type calcium channel
I_{CaK}	potassium current through the L-type calcium channel

I_{ClCa}	calcium-activated chloride current
I_{BCl}	background chloride current
I_{NaL}	late sodium current

References

1. Nattel, S.; Heijman, J.; Zhou, L.; Dobrev, D., Molecular Basis of Atrial Fibrillation Pathophysiology and Therapy: A Translational Perspective. *Circulation research* **2020,** 127, (1), 51-72.
2. van Ouwerkerk, A. F.; Hall, A. W.; Kadow, Z. A.; Lazarevic, S.; Reyat, J. S.; Tucker, N. R.; Nadadur, R. D.; Bosada, F. M.; Bianchi, V.; Ellinor, P. T.; Fabritz, L.; Martin, J. F.; de Laat, W.; Kirchhof, P.; Moskowitz, I. P.; Christoffels, V. M., Epigenetic and Transcriptional Networks Underlying Atrial Fibrillation. *Circulation research* **2020,** 127, (1), 34-50.
3. Benjamin, E. J.; Rice, K. M.; Arking, D. E.; Pfeufer, A.; van Noord, C.; Smith, A. V.; Schnabel, R. B.; Bis, J. C.; Boerwinkle, E.; Sinner, M. F.; Dehghan, A.; Lubitz, S. A.; D'Agostino, R. B., Sr.; Lumley, T.; Ehret, G. B.; Heeringa, J.; Aspelund, T.; Newton-Cheh, C.; Larson, M. G.; Marciante, K. D.; Soliman, E. Z.; Rivadeneira, F.; Wang, T. J.; Eiríksdottir, G.; Levy, D.; Psaty, B. M.; Li, M.; Chamberlain, A. M.; Hofman, A.; Vasan, R. S.; Harris, T. B.; Rotter, J. I.; Kao, W. H.; Agarwal, S. K.; Stricker, B. H.; Wang, K.; Launer, L. J.; Smith, N. L.; Chakravarti, A.; Uitterlinden, A. G.; Wolf, P. A.; Sotoodehnia, N.; Köttgen, A.; van Duijn, C. M.; Meitinger, T.; Mueller, M.; Perz, S.; Steinbeck, G.; Wichmann, H. E.; Lunetta, K. L.; Heckbert, S. R.; Gudnason, V.; Alonso, A.; Kääb, S.; Ellinor, P. T.; Witteman, J. C., Variants in ZFHX3 are associated with atrial fibrillation in individuals of European ancestry. *Nature genetics* **2009,** 41, (8), 879-81.
4. Christophersen, I. E.; Rienstra, M.; Roselli, C.; Yin, X.; Geelhoed, B.; Barnard, J.; Lin, H.; Arking, D. E.; Smith, A. V.; Albert, C. M.; Chaffin, M.; Tucker, N. R.; Li, M.; Klarin, D.; Bihlmeyer, N. A.; Low, S. K.; Weeke, P. E.; Müller-Nurasyid, M.; Smith, J. G.; Brody, J. A.; Niemeijer, M. N.; Dörr, M.; Trompet, S.; Huffman, J.; Gustafsson, S.; Schurmann, C.; Kleber, M. E.; Lyytikäinen, L. P.; Seppälä, I.; Malik, R.; Horimoto, A.; Perez, M.; Sinisalo, J.; Aeschbacher, S.; Thériault, S.; Yao, J.; Radmanesh, F.; Weiss, S.; Teumer, A.; Choi, S. H.; Weng, L. C.; Clauss, S.; Deo, R.; Rader, D. J.; Shah, S. H.; Sun, A.; Hopewell, J. C.; Debette, S.; Chauhan, G.; Yang, Q.; Worrall, B. B.; Paré, G.; Kamatani, Y.; Hagemeijer, Y. P.; Verweij, N.; Siland, J. E.; Kubo, M.; Smith, J. D.; Van Wagoner, D. R.; Bis, J. C.; Perz, S.; Psaty, B. M.; Ridker, P. M.; Magnani, J. W.; Harris, T. B.; Launer, L. J.; Shoemaker, M. B.; Padmanabhan, S.; Haessler, J.; Bartz, T. M.; Waldenberger, M.; Lichtner, P.; Arendt, M.; Krieger, J. E.; Kähönen, M.; Risch, L.; Mansur, A. J.; Peters, A.; Smith, B. H.; Lind, L.; Scott, S. A.; Lu, Y.; Bottinger, E. B.; Hernesniemi, J.; Lindgren, C. M.; Wong, J. A.; Huang, J.; Eskola, M.; Morris, A. P.; Ford, I.; Reiner, A. P.; Delgado, G.; Chen, L. Y.; Chen, Y. I.; Sandhu, R. K.; Li, M.; Boerwinkle, E.; Eisele, L.; Lannfelt, L.; Rost, N.; Anderson, C. D.; Taylor, K. D.; Campbell, A.; Magnusson, P. K.; Porteous, D.; Hocking, L. J.; Vlachopoulou, E.; Pedersen, N. L.; Nikus, K.; Orho-Melander, M.; Hamsten, A.; Heeringa, J.; Denny, J. C.; Kriebel, J.; Darbar, D.; Newton-Cheh, C.; Shaffer, C.; Macfarlane, P. W.; Heilmann-Heimbach, S.; Almgren, P.; Huang, P. L.; Sotoodehnia, N.; Soliman, E. Z.; Uitterlinden, A. G.; Hofman, A.; Franco, O. H.; Völker, U.; Jöckel, K. H.; Sinner, M. F.; Lin, H. J.; Guo, X.; Dichgans, M.; Ingelsson, E.; Kooperberg, C.; Melander, O.; Loos, R. J. F.; Laurikka, J.; Conen, D.; Rosand, J.; van der Harst, P.; Lokki, M. L.; Kathiresan, S.; Pereira, A.; Jukema, J. W.; Hayward, C.; Rotter, J. I.; März, W.; Lehtimäki, T.; Stricker, B. H.; Chung, M. K.; Felix, S. B.; Gudnason, V.; Alonso, A.; Roden, D. M.; Kääb, S.; Chasman, D. I.; Heckbert, S. R.; Benjamin, E. J.; Tanaka, T.; Lunetta, K. L.; Lubitz, S. A.; Ellinor, P. T., Large-scale analyses of common and rare variants identify 12 new loci associated with atrial fibrillation. *Nature genetics* **2017,** 49, (6), 946-952.

5. Ellinor, P. T.; Lunetta, K. L.; Albert, C. M.; Glazer, N. L.; Ritchie, M. D.; Smith, A. V.; Arking, D. E.; Müller-Nurasyid, M.; Krijthe, B. P.; Lubitz, S. A.; Bis, J. C.; Chung, M. K.; Dörr, M.; Ozaki, K.; Roberts, J. D.; Smith, J. G.; Pfeufer, A.; Sinner, M. F.; Lohman, K.; Ding, J.; Smith, N. L.; Smith, J. D.; Rienstra, M.; Rice, K. M.; Van Wagoner, D. R.; Magnani, J. W.; Wakili, R.; Clauss, S.; Rotter, J. I.; Steinbeck, G.; Launer, L. J.; Davies, R. W.; Borkovich, M.; Harris, T. B.; Lin, H.; Völker, U.; Völzke, H.; Milan, D. J.; Hofman, A.; Boerwinkle, E.; Chen, L. Y.; Soliman, E. Z.; Voight, B. F.; Li, G.; Chakravarti, A.; Kubo, M.; Tedrow, U. B.; Rose, L. M.; Ridker, P. M.; Conen, D.; Tsunoda, T.; Furukawa, T.; Sotoodehnia, N.; Xu, S.; Kamatani, N.; Levy, D.; Nakamura, Y.; Parvez, B.; Mahida, S.; Furie, K. L.; Rosand, J.; Muhammad, R.; Psaty, B. M.; Meitinger, T.; Perz, S.; Wichmann, H. E.; Witteman, J. C.; Kao, W. H.; Kathiresan, S.; Roden, D. M.; Uitterlinden, A. G.; Rivadeneira, F.; McKnight, B.; Sjögren, M.; Newman, A. B.; Liu, Y.; Gollob, M. H.; Melander, O.; Tanaka, T.; Stricker, B. H.; Felix, S. B.; Alonso, A.; Darbar, D.; Barnard, J.; Chasman, D. I.; Heckbert, S. R.; Benjamin, E. J.; Gudnason, V.; Kääb, S., Meta-analysis identifies six new susceptibility loci for atrial fibrillation. *Nature genetics* **2012,** 44, (6), 670-5.

6. Ellinor, P. T.; Lunetta, K. L.; Glazer, N. L.; Pfeufer, A.; Alonso, A.; Chung, M. K.; Sinner, M. F.; de Bakker, P. I.; Mueller, M.; Lubitz, S. A.; Fox, E.; Darbar, D.; Smith, N. L.; Smith, J. D.; Schnabel, R. B.; Soliman, E. Z.; Rice, K. M.; Van Wagoner, D. R.; Beckmann, B. M.; van Noord, C.; Wang, K.; Ehret, G. B.; Rotter, J. I.; Hazen, S. L.; Steinbeck, G.; Smith, A. V.; Launer, L. J.; Harris, T. B.; Makino, S.; Nelis, M.; Milan, D. J.; Perz, S.; Esko, T.; Köttgen, A.; Moebus, S.; Newton-Cheh, C.; Li, M.; Möhlenkamp, S.; Wang, T. J.; Kao, W. H.; Vasan, R. S.; Nöthen, M. M.; MacRae, C. A.; Stricker, B. H.; Hofman, A.; Uitterlinden, A. G.; Levy, D.; Boerwinkle, E.; Metspalu, A.; Topol, E. J.; Chakravarti, A.; Gudnason, V.; Psaty, B. M.; Roden, D. M.; Meitinger, T.; Wichmann, H. E.; Witteman, J. C.; Barnard, J.; Arking, D. E.; Benjamin, E. J.; Heckbert, S. R.; Kääb, S., Common variants in KCNN3 are associated with lone atrial fibrillation. *Nature genetics* **2010,** 42, (3), 240-4.

7. Low, S. K.; Takahashi, A.; Ebana, Y.; Ozaki, K.; Christophersen, I. E.; Ellinor, P. T.; Ogishima, S.; Yamamoto, M.; Satoh, M.; Sasaki, M.; Yamaji, T.; Iwasaki, M.; Tsugane, S.; Tanaka, K.; Naito, M.; Wakai, K.; Tanaka, H.; Furukawa, T.; Kubo, M.; Ito, K.; Kamatani, Y.; Tanaka, T., Identification of six new genetic loci associated with atrial fibrillation in the Japanese population. *Nature genetics* **2017,** 49, (6), 953-958.

8. Roselli, C.; Chaffin, M. D.; Weng, L. C.; Aeschbacher, S.; Ahlberg, G.; Albert, C. M.; Almgren, P.; Alonso, A.; Anderson, C. D.; Aragam, K. G.; Arking, D. E.; Barnard, J.; Bartz, T. M.; Benjamin, E. J.; Bihlmeyer, N. A.; Bis, J. C.; Bloom, H. L.; Boerwinkle, E.; Bottinger, E. B.; Brody, J. A.; Calkins, H.; Campbell, A.; Cappola, T. P.; Carlquist, J.; Chasman, D. I.; Chen, L. Y.; Chen, Y. I.; Choi, E. K.; Choi, S. H.; Christophersen, I. E.; Chung, M. K.; Cole, J. W.; Conen, D.; Cook, J.; Crijns, H. J.; Cutler, M. J.; Damrauer, S. M.; Daniels, B. R.; Darbar, D.; Delgado, G.; Denny, J. C.; Dichgans, M.; Dörr, M.; Dudink, E. A.; Dudley, S. C.; Esa, N.; Esko, T.; Eskola, M.; Fatkin, D.; Felix, S. B.; Ford, I.; Franco, O. H.; Geelhoed, B.; Grewal, R. P.; Gudnason, V.; Guo, X.; Gupta, N.; Gustafsson, S.; Gutmann, R.; Hamsten, A.; Harris, T. B.; Hayward, C.; Heckbert, S. R.; Hernesniemi, J.; Hocking, L. J.; Hofman, A.; Horimoto, A.; Huang, J.; Huang, P. L.; Huffman, J.; Ingelsson, E.; Ipek, E. G.; Ito, K.; Jimenez-Conde, J.; Johnson, R.; Jukema, J. W.; Kääb, S.; Kähönen, M.; Kamatani, Y.; Kane, J. P.; Kastrati, A.; Kathiresan, S.; Katschnig-Winter, P.; Kavousi, M.; Kessler, T.; Kietselaer, B. L.; Kirchhof, P.; Kleber, M. E.; Knight, S.; Krieger, J. E.; Kubo, M.; Launer, L. J.; Laurikka, J.; Lehtimäki, T.; Leineweber, K.; Lemaitre, R. N.; Li, M.; Lim, H. E.; Lin, H. J.; Lin, H.; Lind, L.; Lindgren, C. M.; Lokki, M. L.; London, B.; Loos, R. J. F.; Low, S. K.; Lu, Y.; Lyytikäinen, L. P.; Macfarlane, P. W.; Magnusson, P. K.; Mahajan, A.; Malik, R.; Mansur, A. J.; Marcus, G. M.;

Margolin, L.; Margulies, K. B.; März, W.; McManus, D. D.; Melander, O.; Mohanty, S.; Montgomery, J. A.; Morley, M. P.; Morris, A. P.; Müller-Nurasyid, M.; Natale, A.; Nazarian, S.; Neumann, B.; Newton-Cheh, C.; Niemeijer, M. N.; Nikus, K.; Nilsson, P.; Noordam, R.; Oellers, H.; Olesen, M. S.; Orho-Melander, M.; Padmanabhan, S.; Pak, H. N.; Paré, G.; Pedersen, N. L.; Pera, J.; Pereira, A.; Porteous, D.; Psaty, B. M.; Pulit, S. L.; Pullinger, C. R.; Rader, D. J.; Refsgaard, L.; Ribasés, M.; Ridker, P. M.; Rienstra, M.; Risch, L.; Roden, D. M.; Rosand, J.; Rosenberg, M. A.; Rost, N.; Rotter, J. I.; Saba, S.; Sandhu, R. K.; Schnabel, R. B.; Schramm, K.; Schunkert, H.; Schurman, C.; Scott, S. A.; Seppälä, I.; Shaffer, C.; Shah, S.; Shalaby, A. A.; Shim, J.; Shoemaker, M. B.; Siland, J. E.; Sinisalo, J.; Sinner, M. F.; Slowik, A.; Smith, A. V.; Smith, B. H.; Smith, J. G.; Smith, J. D.; Smith, N. L.; Soliman, E. Z.; Sotoodehnia, N.; Stricker, B. H.; Sun, A.; Sun, H.; Svendsen, J. H.; Tanaka, T.; Tanriverdi, K.; Taylor, K. D.; Teder-Laving, M.; Teumer, A.; Thériault, S.; Trompet, S.; Tucker, N. R.; Tveit, A.; Uitterlinden, A. G.; Van Der Harst, P.; Van Gelder, I. C.; Van Wagoner, D. R.; Verweij, N.; Vlachopoulou, E.; Völker, U.; Wang, B.; Weeke, P. E.; Weijs, B.; Weiss, R.; Weiss, S.; Wells, Q. S.; Wiggins, K. L.; Wong, J. A.; Woo, D.; Worrall, B. B.; Yang, P. S.; Yao, J.; Yoneda, Z. T.; Zeller, T.; Zeng, L.; Lubitz, S. A.; Lunetta, K. L.; Ellinor, P. T., Multi-ethnic genome-wide association study for atrial fibrillation. *Nature genetics* **2018,** 50, (9), 1225-1233.

9. Sinner, M. F.; Tucker, N. R.; Lunetta, K. L.; Ozaki, K.; Smith, J. G.; Trompet, S.; Bis, J. C.; Lin, H.; Chung, M. K.; Nielsen, J. B.; Lubitz, S. A.; Krijthe, B. P.; Magnani, J. W.; Ye, J.; Gollob, M. H.; Tsunoda, T.; Müller-Nurasyid, M.; Lichtner, P.; Peters, A.; Dolmatova, E.; Kubo, M.; Smith, J. D.; Psaty, B. M.; Smith, N. L.; Jukema, J. W.; Chasman, D. I.; Albert, C. M.; Ebana, Y.; Furukawa, T.; Macfarlane, P. W.; Harris, T. B.; Darbar, D.; Dörr, M.; Holst, A. G.; Svendsen, J. H.; Hofman, A.; Uitterlinden, A. G.; Gudnason, V.; Isobe, M.; Malik, R.; Dichgans, M.; Rosand, J.; Van Wagoner, D. R.; Benjamin, E. J.; Milan, D. J.; Melander, O.; Heckbert, S. R.; Ford, I.; Liu, Y.; Barnard, J.; Olesen, M. S.; Stricker, B. H.; Tanaka, T.; Kääb, S.; Ellinor, P. T., Integrating genetic, transcriptional, and functional analyses to identify 5 novel genes for atrial fibrillation. *Circulation* **2014,** 130, (15), 1225-35.

10. Gudbjartsson, D. F.; Arnar, D. O.; Helgadottir, A.; Gretarsdottir, S.; Holm, H.; Sigurdsson, A.; Jonasdottir, A.; Baker, A.; Thorleifsson, G.; Kristjansson, K.; Palsson, A.; Blondal, T.; Sulem, P.; Backman, V. M.; Hardarson, G. A.; Palsdottir, E.; Helgason, A.; Sigurjonsdottir, R.; Sverrisson, J. T.; Kostulas, K.; Ng, M. C.; Baum, L.; So, W. Y.; Wong, K. S.; Chan, J. C.; Furie, K. L.; Greenberg, S. M.; Sale, M.; Kelly, P.; MacRae, C. A.; Smith, E. E.; Rosand, J.; Hillert, J.; Ma, R. C.; Ellinor, P. T.; Thorgeirsson, G.; Gulcher, J. R.; Kong, A.; Thorsteinsdottir, U.; Stefansson, K., Variants conferring risk of atrial fibrillation on chromosome 4q25. *Nature* **2007,** 448, (7151), 353-7.

11. Kirchhof, P.; Kahr, P. C.; Kaese, S.; Piccini, I.; Vokshi, I.; Scheld, H. H.; Rotering, H.; Fortmueller, L.; Laakmann, S.; Verheule, S.; Schotten, U.; Fabritz, L.; Brown, N. A., PITX2c is expressed in the adult left atrium, and reducing Pitx2c expression promotes atrial fibrillation inducibility and complex changes in gene expression. *Circulation. Cardiovascular genetics* **2011,** 4, (2), 123-33.

12. Tao, Y.; Zhang, M.; Li, L.; Bai, Y.; Zhou, Y.; Moon, A. M.; Kaminski, H. J.; Martin, J. F., Pitx2, an atrial fibrillation predisposition gene, directly regulates ion transport and intercalated disc genes. *Circulation. Cardiovascular genetics* **2014,** 7, (1), 23-32.

13. Mommersteeg, M. T.; Brown, N. A.; Prall, O. W.; de Gier-de Vries, C.; Harvey, R. P.; Moorman, A. F.; Christoffels, V. M., Pitx2c and Nkx2-5 are required for the formation and identity of the pulmonary myocardium. *Circulation research* **2007,** 101, (9), 902-9.

14. Ye, J.; Tucker, N. R.; Weng, L. C.; Clauss, S.; Lubitz, S. A.; Ellinor, P. T., A Functional Variant Associated with Atrial Fibrillation Regulates PITX2c Expression through TFAP2a. *American journal of human genetics* **2016,** 99, (6), 1281-1291.
15. Wang, J.; Klysik, E.; Sood, S.; Johnson, R. L.; Wehrens, X. H.; Martin, J. F., Pitx2 prevents susceptibility to atrial arrhythmias by inhibiting left-sided pacemaker specification. *Proceedings of the National Academy of Sciences of the United States of America* **2010,** 107, (21), 9753-8.
16. Aguirre, L. A.; Alonso, M. E.; Badía-Careaga, C.; Rollán, I.; Arias, C.; Fernández-Miñán, A.; López-Jiménez, E.; Aránega, A.; Gómez-Skarmeta, J. L.; Franco, D.; Manzanares, M., Long-range regulatory interactions at the 4q25 atrial fibrillation risk locus involve PITX2c and ENPEP. *BMC biology* **2015,** 13, 26.
17. Nadadur, R. D.; Broman, M. T.; Boukens, B.; Mazurek, S. R.; Yang, X.; van den Boogaard, M.; Bekeny, J.; Gadek, M.; Ward, T.; Zhang, M.; Qiao, Y.; Martin, J. F.; Seidman, C. E.; Seidman, J.; Christoffels, V.; Efimov, I. R.; McNally, E. M.; Weber, C. R.; Moskowitz, I. P., Pitx2 modulates a Tbx5-dependent gene regulatory network to maintain atrial rhythm. *Science translational medicine* **2016,** 8, (354), 354ra115.
18. Syeda, F.; Holmes, A. P.; Yu, T. Y.; Tull, S.; Kuhlmann, S. M.; Pavlovic, D.; Betney, D.; Riley, G.; Kucera, J. P.; Jousset, F.; de Groot, J. R.; Rohr, S.; Brown, N. A.; Fabritz, L.; Kirchhof, P., PITX2 Modulates Atrial Membrane Potential and the Antiarrhythmic Effects of Sodium-Channel Blockers. *Journal of the American College of Cardiology* **2016,** 68, (17), 1881-1894.
19. Zhang, M.; Hill, M. C.; Kadow, Z. A.; Suh, J. H.; Tucker, N. R.; Hall, A. W.; Tran, T. T.; Swinton, P. S.; Leach, J. P.; Margulies, K. B.; Ellinor, P. T.; Li, N.; Martin, J. F., Long-range Pitx2c enhancer-promoter interactions prevent predisposition to atrial fibrillation. *Proceedings of the National Academy of Sciences of the United States of America* **2019,** 116, (45), 22692-22698.
20. Reyat, J. S.; Chua, W.; Cardoso, V. R.; Witten, A.; Kastner, P. M.; Kabir, S. N.; Sinner, M. F.; Wesselink, R.; Holmes, A. P.; Pavlovic, D.; Stoll, M.; Kääb, S.; Gkoutos, G. V.; de Groot, J. R.; Kirchhof, P.; Fabritz, L., Reduced left atrial cardiomyocyte PITX2 and elevated circulating BMP10 predict atrial fibrillation after ablation. *JCI insight* **2020,** 5, (16).
21. Mommersteeg, M. T.; Hoogaars, W. M.; Prall, O. W.; de Gier-de Vries, C.; Wiese, C.; Clout, D. E.; Papaioannou, V. E.; Brown, N. A.; Harvey, R. P.; Moorman, A. F.; Christoffels, V. M., Molecular pathway for the localized formation of the sinoatrial node. *Circulation research* **2007,** 100, (3), 354-62.
22. Chinchilla, A.; Daimi, H.; Lozano-Velasco, E.; Dominguez, J. N.; Caballero, R.; Delpón, E.; Tamargo, J.; Cinca, J.; Hove-Madsen, L.; Aranega, A. E.; Franco, D., PITX2 insufficiency leads to atrial electrical and structural remodeling linked to arrhythmogenesis. *Circulation. Cardiovascular genetics* **2011,** 4, (3), 269-79.
23. Lozano-Velasco, E.; Hernández-Torres, F.; Daimi, H.; Serra, S. A.; Herraiz, A.; Hove-Madsen, L.; Aránega, A.; Franco, D., Pitx2 impairs calcium handling in a dose-dependent manner by modulating Wnt signalling. *Cardiovascular research* **2016,** 109, (1), 55-66.
24. Herraiz-Martínez, A.; Llach, A.; Tarifa, C.; Gandía, J.; Jiménez-Sabado, V.; Lozano-Velasco, E.; Serra, S. A.; Vallmitjana, A.; Vázquez Ruiz de Castroviejo, E.; Benítez, R.; Aranega, A.; Muñoz-Guijosa, C.; Franco, D.; Cinca, J.; Hove-Madsen, L., The 4q25 variant rs13143308T links risk of atrial fibrillation to defective calcium homoeostasis. *Cardiovascular research* **2019,** 115, (3), 578-589.
25. Lozano-Velasco, E.; Wangensteen, R.; Quesada, A.; Garcia-Padilla, C.; Osorio, J. A.; Ruiz-Torres, M. D.; Aranega, A.; Franco, D., Hyperthyroidism, but not hypertension, impairs PITX2 expression leading to Wnt-microRNA-ion channel remodeling. *PloS one* **2017,** 12, (12), e0188473.

26. Pérez-Hernández, M.; Matamoros, M.; Barana, A.; Amorós, I.; Gómez, R.; Núñez, M.; Sacristán, S.; Pinto, Á.; Fernández-Avilés, F.; Tamargo, J.; Delpón, E.; Caballero, R., Pitx2c increases in atrial myocytes from chronic atrial fibrillation patients enhancing IKs and decreasing ICa,L. *Cardiovascular research* **2016,** 109, (3), 431-41.
27. Bai, J.; Gladding, P. A.; Stiles, M. K.; Fedorov, V. V.; Zhao, J., Ionic and cellular mechanisms underlying TBX5/PITX2 insufficiency-induced atrial fibrillation: Insights from mathematical models of human atrial cells. *Scientific Reports* **2018,** 8, (1), 15642.
28. Bai, J.; Lu, Y.; Lo, A.; Zhao, J. In *PITX2 Overexpression Leads to Atrial Electrical Remodeling Linked to Atrial Fibrillation*, 2019 Computing in Cardiology (CinC), 8-11 Sept. 2019, 2019; 2019; pp Page1-Page4.
29. Bai, J.; Lu, Y.; Lo, A.; Zhao, J.; Zhang, H., Proarrhythmia in the p.Met207Val PITX2c-Linked Familial Atrial Fibrillation-Insights From Modeling. *Frontiers in physiology* **2019,** 10, 1314.
30. Bai, J.; Lu, Y.; Lo, A.; Zhao, J.; Zhang, H., PITX2 upregulation increases the risk of chronic atrial fibrillation in a dose-dependent manner by modulating I(Ks) and I(CaL) -insights from human atrial modelling. *Annals of translational medicine* **2020,** 8, (5), 191.
31. Bai, J.; Lu, Y.; Zhang, H., In silico study of the effects of anti-arrhythmic drug treatment on sinoatrial node function for patients with atrial fibrillation. *Sci Rep* **2020,** 10, (1), 305.
32. Bai, J.; Zhu, Y.; Lo, A.; Lu, Y.; Zhao, J., In Silico Assessment of Genetic Variation in PITX2 Reveals the Molecular Mechanisms of Calcium-Mediated Cellular Triggered Activity in Atrial Fibrillation(). *Annual International Conference of the IEEE Engineering in Medicine and Biology Society. IEEE Engineering in Medicine and Biology Society. Annual International Conference* **2020,** 2020, 2353-2356.
33. Zhu, Y.; Bai, J.; Lo, A.; Lu, Y.; Zhao, J., Mechanisms underlying pro-arrhythmic abnormalities arising from Pitx2-induced electrical remodelling: An in silico intersubject variability study. *Annals of translational medicine* **2020,** In Press.
34. Parvez, B.; Vaglio, J.; Rowan, S.; Muhammad, R.; Kucera, G.; Stubblefield, T.; Carter, S.; Roden, D.; Darbar, D., Symptomatic response to antiarrhythmic drug therapy is modulated by a common single nucleotide polymorphism in atrial fibrillation. *Journal of the American College of Cardiology* **2012,** 60, (6), 539-45.
35. Ang, Y. S.; Rajamani, S.; Haldar, S. M.; Hüser, J., A New Therapeutic Framework for Atrial Fibrillation Drug Development. *Circulation research* **2020,** 127, (1), 184-201.
36. Bai, J.; Lo, A.; Gladding, P. A.; Stiles, M. K.; Fedorov, V. V.; Zhao, J., In silico investigation of the mechanisms underlying atrial fibrillation due to impaired Pitx2. *PLoS computational biology* **2020,** 16, (2), e1007678.
37. Whittaker, D. G.; Hancox, J. C.; Zhang, H., In silico Assessment of Pharmacotherapy for Human Atrial Patho-Electrophysiology Associated With hERG-Linked Short QT Syndrome. *Frontiers in physiology* **2018,** 9, 1888.
38. Paci, M.; Casini, S.; Bellin, M.; Hyttinen, J.; Severi, S., Large-Scale Simulation of the Phenotypical Variability Induced by Loss-of-Function Long QT Mutations in Human Induced Pluripotent Stem Cell Cardiomyocytes. *International journal of molecular sciences* **2018,** 19, (11).
39. Kernik, D. C.; Yang, P. C.; Kurokawa, J.; Wu, J. C.; Clancy, C. E., A computational model of induced pluripotent stem-cell derived cardiomyocytes for high throughput risk stratification of KCNQ1 genetic variants. *PLoS computational biology* **2020,** 16, (8), e1008109.
40. Kernik, D. C.; Morotti, S.; Wu, H.; Garg, P.; Duff, H. J.; Kurokawa, J.; Jalife, J.; Wu, J. C.; Grandi, E.; Clancy, C. E., A computational model of induced pluripotent stem-cell derived cardiomyocytes

incorporating experimental variability from multiple data sources. *The Journal of physiology* **2019,** 597, (17), 4533-4564.

41. Sobie, E. A., Parameter sensitivity analysis in electrophysiological models using multivariable regression. *Biophysical journal* **2009,** 96, (4), 1264-74.
42. Sarkar, A. X.; Sobie, E. A., Quantification of repolarization reserve to understand interpatient variability in the response to proarrhythmic drugs: a computational analysis. *Heart rhythm* **2011,** 8, (11), 1749-55.
43. Cummins, M. A.; Dalal, P. J.; Bugana, M.; Severi, S.; Sobie, E. A., Comprehensive analyses of ventricular myocyte models identify targets exhibiting favorable rate dependence. *PLoS computational biology* **2014,** 10, (3), e1003543.
44. Morotti, S.; Grandi, E., Logistic regression analysis of populations of electrophysiological models to assess proarrythmic risk. *MethodsX* **2017,** 4, 25-34.
45. Passini, E.; Britton, O. J.; Lu, H. R.; Rohrbacher, J.; Hermans, A. N.; Gallacher, D. J.; Greig, R. J. H.; Bueno-Orovio, A.; Rodriguez, B., Human In Silico Drug Trials Demonstrate Higher Accuracy than Animal Models in Predicting Clinical Pro-Arrhythmic Cardiotoxicity. *Frontiers in physiology* **2017,** 8, 668.
46. Romero, L.; Pueyo, E.; Fink, M.; Rodríguez, B., Impact of ionic current variability on human ventricular cellular electrophysiology. *American journal of physiology. Heart and circulatory physiology* **2009,** 297, (4), H1436-45.
47. Sarkar, A. X.; Christini, D. J.; Sobie, E. A., Exploiting mathematical models to illuminate electrophysiological variability between individuals. *The Journal of physiology* **2012,** 590, (11), 2555-67.
48. Pueyo, E.; Corrias, A.; Virág, L.; Jost, N.; Szél, T.; Varró, A.; Szentandrássy, N.; Nánási, P. P.; Burrage, K.; Rodríguez, B., A multiscale investigation of repolarization variability and its role in cardiac arrhythmogenesis. *Biophysical journal* **2011,** 101, (12), 2892-902.
49. Gotta, V.; Cools, F.; van Ammel, K.; Gallacher, D. J.; Visser, S. A.; Sannajust, F.; Morissette, P.; Danhof, M.; van der Graaf, P. H., Inter-study variability of preclinical in vivo safety studies and translational exposure-QTc relationships--a PKPD meta-analysis. *British journal of pharmacology* **2015,** 172, (17), 4364-79.
50. Britton, O. J.; Bueno-Orovio, A.; Van Ammel, K.; Lu, H. R.; Towart, R.; Gallacher, D. J.; Rodriguez, B., Experimentally calibrated population of models predicts and explains intersubject variability in cardiac cellular electrophysiology. *Proceedings of the National Academy of Sciences of the United States of America* **2013,** 110, (23), E2098-105.
51. Muszkiewicz, A.; Liu, X.; Bueno-Orovio, A.; Lawson, B. A. J.; Burrage, K.; Casadei, B.; Rodriguez, B., From ionic to cellular variability in human atrial myocytes: an integrative computational and experimental study. *American journal of physiology. Heart and circulatory physiology* **2018,** 314, (5), H895-h916.
52. Gong, J. Q. X.; Sobie, E. A., Population-based mechanistic modeling allows for quantitative predictions of drug responses across cell types. *NPJ systems biology and applications* **2018,** 4, 11.
53. Rieger, T. R.; Allen, R. J.; Bystricky, L.; Chen, Y.; Colopy, G. W.; Cui, Y.; Gonzalez, A.; Liu, Y.; White, R. D.; Everett, R. A.; Banks, H. T.; Musante, C. J., Improving the generation and selection of virtual populations in quantitative systems pharmacology models. *Prog Biophys Mol Biol* **2018,** 139, 15-22.
54. Muszkiewicz, A.; Britton, O. J.; Gemmell, P.; Passini, E.; Sánchez, C.; Zhou, X.; Carusi, A.; Quinn, T. A.; Burrage, K.; Bueno-Orovio, A.; Rodriguez, B., Variability in cardiac electrophysiology: Using experimentally-calibrated populations of models to move beyond the single virtual physiological human paradigm. *Progress in Biophysics and Molecular Biology* **2016,** 120, (1), 115-127.

55. Ni, H.; Iseppe, A. F.; Giles, W. R.; Narayan, S. M.; Zhang, H.; Edwards, A. G.; Morotti, S.; Grandi, E., Populations of in silico myocytes and tissues reveal synergy of multi-atrial-predominant K(+) -current block in atrial fibrillation. *British journal of pharmacology* **2020,** 177, (19), 4497-515.
56. Vagos, M. R.; Arevalo, H.; de Oliveira, B. L.; Sundnes, J.; Maleckar, M. M., A computational framework for testing arrhythmia marker sensitivities to model parameters in functionally calibrated populations of atrial cells. *Chaos (Woodbury, N.Y.)* **2017,** 27, (9), 093941.
57. Lawson, B. A. J.; Drovandi, C. C.; Cusimano, N.; Burrage, P.; Rodriguez, B.; Burrage, K., Unlocking data sets by calibrating populations of models to data density: A study in atrial electrophysiology. *Science advances* **2018,** 4, (1), e1701676.
58. Ni, H.; Morotti, S.; Grandi, E., A Heart for Diversity: Simulating Variability in Cardiac Arrhythmia Research. *Frontiers in physiology* **2018,** 9, 958.
59. Ravens, U.; Katircioglu-Öztürk, D.; Wettwer, E.; Christ, T.; Dobrev, D.; Voigt, N.; Poulet, C.; Loose, S.; Simon, J.; Stein, A.; Matschke, K.; Knaut, M.; Oto, E.; Oto, A.; Güvenir, H. A., Application of the RIMARC algorithm to a large data set of action potentials and clinical parameters for risk prediction of atrial fibrillation. *Medical & biological engineering & computing* **2015,** 53, (3), 263-73.
60. Grandi, E.; Pandit, S. V.; Voigt, N.; Workman, A. J.; Dobrev, D.; Jalife, J.; Bers, D. M., Human atrial action potential and Ca2+ model: sinus rhythm and chronic atrial fibrillation. *Circulation research* **2011,** 109, (9), 1055-66.
61. Mechakra, A.; Footz, T.; Walter, M.; Aránega, A.; Hernández-Torres, F.; Morel, E.; Millat, G.; Yang, Y. Q.; Chahine, M.; Chevalier, P.; Christé, G., A Novel PITX2c Gain-of-Function Mutation, p.Met207Val, in Patients With Familial Atrial Fibrillation. *The American journal of cardiology* **2019,** 123, (5), 787-793.
62. Wang, Z.; Fermini, B.; Nattel, S., Delayed rectifier outward current and repolarization in human atrial myocytes. *Circulation research* **1993,** 73, (2), 276-85.
63. Ellinwood, N.; Dobrev, D.; Morotti, S.; Grandi, E., In Silico Assessment of Efficacy and Safety of I(Kur) Inhibitors in Chronic Atrial Fibrillation: Role of Kinetics and State-Dependence of Drug Binding. *Frontiers in pharmacology* **2017,** 8, 799.
64. Grandi, E.; Maleckar, M. M., Anti-arrhythmic strategies for atrial fibrillation: The role of computational modeling in discovery, development, and optimization. *Pharmacology & therapeutics* **2016,** 168, 126-142.
65. Kramer, J.; Obejero-Paz, C. A.; Myatt, G.; Kuryshev, Y. A.; Bruening-Wright, A.; Verducci, J. S.; Brown, A. M., MICE models: superior to the HERG model in predicting Torsade de Pointes. *Sci Rep* **2013,** 3, 2100.
66. Zhang, H.; Zou, B.; Du, F.; Xu, K.; Li, M., Reporting sodium channel activity using calcium flux: pharmacological promiscuity of cardiac Nav1.5. *Molecular pharmacology* **2015,** 87, (2), 207-17.
67. Zhang, Y. H.; Hancox, J. C., Mode-dependent inhibition by quinidine of Na+-Ca2+ exchanger current from guinea-pig isolated ventricular myocytes. *Clinical and experimental pharmacology & physiology* **2002,** 29, (9), 777-81.
68. Hancox, J. C.; Mitcheson, J. S., Inhibition of L-type calcium current by propafenone in single myocytes isolated from the rabbit atrioventricular node. *British journal of pharmacology* **1997,** 121, (1), 7-14.
69. Hanada, E.; Ohtani, H.; Hirota, M.; Uemura, N.; Nakaya, H.; Kotaki, H.; Sato, H.; Yamada, Y.; Iga, T., Inhibitory effect of erythromycin on potassium currents in rat ventricular myocytes in comparison with disopyramide. *The Journal of pharmacy and pharmacology* **2003,** 55, (7), 995-1002.

70. Nenov, N. I.; Crumb, W. J., Jr.; Pigott, J. D.; Harrison, L. H., Jr.; Clarkson, C. W., Quinidine interactions with human atrial potassium channels: developmental aspects. *Circulation research* **1998,** 83, (12), 1224-31.
71. Gross, G. J.; Castle, N. A., Propafenone inhibition of human atrial myocyte repolarizing currents. *Journal of molecular and cellular cardiology* **1998,** 30, (4), 783-93.
72. Satoh, H., Comparative actions of cibenzoline and disopyramide on I(Kr) and I(Ks) currents in rat sino-atrial nodal cells. *European journal of pharmacology* **2000,** 407, (1-2), 123-9.
73. Kang, J.; Chen, X. L.; Wang, L.; Rampe, D., Interactions of the antimalarial drug mefloquine with the human cardiac potassium channels KvLQT1/minK and HERG. *The Journal of pharmacology and experimental therapeutics* **2001,** 299, (1), 290-6.
74. Katchman, A. N.; Koerner, J.; Tosaka, T.; Woosley, R. L.; Ebert, S. N., Comparative evaluation of HERG currents and QT intervals following challenge with suspected torsadogenic and nontorsadogenic drugs. *The Journal of pharmacology and experimental therapeutics* **2006,** 316, (3), 1098-106.
75. Aréchiga, I. A.; Barrio-Echavarria, G. F.; Rodríguez-Menchaca, A. A.; Moreno-Galindo, E. G.; Decher, N.; Tristani-Firouzi, M.; Sánchez-Chapula, J. A.; Navarro-Polanco, R. A., Kv1.5 open channel block by the antiarrhythmic drug disopyramide: molecular determinants of block. *Journal of pharmacological sciences* **2008,** 108, (1), 49-55.
76. Franqueza, L.; Valenzuela, C.; Delpón, E.; Longobardo, M.; Caballero, R.; Tamargo, J., Effects of propafenone and 5-hydroxy-propafenone on hKv1.5 channels. *British journal of pharmacology* **1998,** 125, (5), 969-78.
77. Amorós, I.; Dolz-Gaitón, P.; Gómez, R.; Matamoros, M.; Barana, A.; de la Fuente, M. G.; Núñez, M.; Pérez-Hernández, M.; Moraleda, I.; Gálvez, E.; Iriepa, I.; Tamargo, J.; Caballero, R.; Delpón, E., Propafenone blocks human cardiac Kir2.x channels by decreasing the negative electrostatic charge in the cytoplasmic pore. *Biochemical pharmacology* **2013,** 86, (2), 267-78.
78. Borchard, U.; Boisten, M., Effect of flecainide on action potentials and alternating current-induced arrhythmias in mammalian myocardium. *Journal of cardiovascular pharmacology* **1982,** 4, (2), 205-12.
79. Kojima, M.; Hamamoto, T.; Ban, T., Sodium channel-blocking properties of flecainide, a class IC antiarrhythmic drug, in guinea-pig papillary muscles. An open channel blocker or an inactivated channel blocker. *Naunyn-Schmiedeberg's archives of pharmacology* **1989,** 339, (4), 441-7.
80. Ferrero, A.; Chorro, F. J.; Cánoves, J.; Mainar, L.; Blasco, E.; Such, L., Effect of flecainide on longitudinal and transverse conduction velocities in ventricular myocardium. An experimental study. *Revista espanola de cardiologia* **2007,** 60, (3), 315-8.
81. O'Shea, C.; Pavlovic, D.; Rajpoot, K.; Winter, J., Examination of the Effects of Conduction Slowing on the Upstroke of Optically Recorded Action Potentials. *Frontiers in physiology* **2019,** 10, 1295.
82. Burton, F. L.; Cobbe, S. M., Dispersion of ventricular repolarization and refractory period. *Cardiovascular research* **2001,** 50, (1), 10-23.
83. Slawsky, M. T.; Castle, N. A., K+ channel blocking actions of flecainide compared with those of propafenone and quinidine in adult rat ventricular myocytes. *The Journal of pharmacology and experimental therapeutics* **1994,** 269, (1), 66-74.
84. Duan, D.; Fermini, B.; Nattel, S., Potassium channel blocking properties of propafenone in rabbit atrial myocytes. *The Journal of pharmacology and experimental therapeutics* **1993,** 264, (3), 1113-23.
85. Seki, A.; Hagiwara, N.; Kasanuki, H., Effects of propafenone on K currents in human atrial myocytes. *British journal of pharmacology* **1999,** 126, (5), 1153-62.

86. Sagawa, K.; Mohri, K.; Shimada, S.; Shimizu, M.; Muramatsu, J., Disopyramide concentrations in human plasma and saliva: comparison of disopyramide concentrations in saliva and plasma unbound concentrations. *European journal of clinical pharmacology* **1997,** 52, (1), 65-9.
87. Whittaker, D. G.; Ni, H.; Benson, A. P.; Hancox, J. C.; Zhang, H., Computational Analysis of the Mode of Action of Disopyramide and Quinidine on hERG-Linked Short QT Syndrome in Human Ventricles. *Frontiers in physiology* **2017,** 8, 759.
88. Wettwer, E.; Hála, O.; Christ, T.; Heubach, J. F.; Dobrev, D.; Knaut, M.; Varró, A.; Ravens, U., Role of IKur in controlling action potential shape and contractility in the human atrium: influence of chronic atrial fibrillation. *Circulation* **2004,** 110, (16), 2299-306.
89. Workman, A. J.; Kane, K. A.; Rankin, A. C., The contribution of ionic currents to changes in refractoriness of human atrial myocytes associated with chronic atrial fibrillation. *Cardiovascular research* **2001,** 52, (2), 226-35.
90. Edwards, A. G.; Louch, W. E., Species-Dependent Mechanisms of Cardiac Arrhythmia: A Cellular Focus. *Clinical Medicine Insights. Cardiology* **2017,** 11, 1179546816686061.
91. Nattel, S.; Dobrev, D., Electrophysiological and molecular mechanisms of paroxysmal atrial fibrillation. *Nature reviews. Cardiology* **2016,** 13, (10), 575-90.
92. Scridon, A.; Fouilloux-Meugnier, E.; Loizon, E.; Rome, S.; Julien, C.; Barrès, C.; Chevalier, P., Long-standing arterial hypertension is associated with Pitx2 down-regulation in a rat model of spontaneous atrial tachyarrhythmias. *Europace : European pacing, arrhythmias, and cardiac electrophysiology : journal of the working groups on cardiac pacing, arrhythmias, and cardiac cellular electrophysiology of the European Society of Cardiology* **2015,** 17, (1), 160-5.
93. Cheng, H.; Cannell, M. B.; Hancox, J. C., Differential responses of rabbit ventricular and atrial transient outward current (I(to)) to the I(to) modulator NS5806. *Physiological reports* **2017,** 5, (5).
94. Vandenberg, J. I.; Varghese, A.; Lu, Y.; Bursill, J. A.; Mahaut-Smith, M. P.; Huang, C. L., Temperature dependence of human ether-a-go-go-related gene K+ currents. *American journal of physiology. Cell physiology* **2006,** 291, (1), C165-75.
95. Grandi, E.; Pasqualini, F. S.; Bers, D. M., A novel computational model of the human ventricular action potential and Ca transient. *Journal of molecular and cellular cardiology* **2010,** 48, (1), 112-21.
96. ten Tusscher, K. H.; Noble, D.; Noble, P. J.; Panfilov, A. V., A model for human ventricular tissue. *American journal of physiology. Heart and circulatory physiology* **2004,** 286, (4), H1573-89.
97. ten Tusscher, K. H.; Panfilov, A. V., Alternans and spiral breakup in a human ventricular tissue model. *American journal of physiology. Heart and circulatory physiology* **2006,** 291, (3), H1088-100.
98. Hansson, A.; Holm, M.; Blomström, P.; Johansson, R.; Lührs, C.; Brandt, J.; Olsson, S. B., Right atrial free wall conduction velocity and degree of anisotropy in patients with stable sinus rhythm studied during open heart surgery. *European heart journal* **1998,** 19, (2), 293-300.
99. Krul, S. P.; Berger, W. R.; Smit, N. W.; van Amersfoorth, S. C.; Driessen, A. H.; van Boven, W. J.; Fiolet, J. W.; van Ginneken, A. C.; van der Wal, A. C.; de Bakker, J. M.; Coronel, R.; de Groot, J. R., Atrial fibrosis and conduction slowing in the left atrial appendage of patients undergoing thoracoscopic surgical pulmonary vein isolation for atrial fibrillation. *Circulation. Arrhythmia and electrophysiology* **2015,** 8, (2), 288-95.
100. Roden, D. M.; Woosley, R. L., Class I antiarrhythmic agents: quinidine, procainamide and N-acetylprocainamide, disopyramide. *Pharmacology & therapeutics* **1983,** 23, (2), 179-91.

101. Britton, O. J.; Bueno-Orovio, A.; Van Ammel, K.; Lu, H. R.; Towart, R.; Gallacher, D. J.; Rodriguez, B., Experimentally calibrated population of models predicts and explains intersubject variability in cardiac cellular electrophysiology. *Proc Natl Acad Sci USA* **2013,** 110, (23), E2098-E2105.

102. Morrison, T. M.; Hariharan, P.; Funkhouser, C. M.; Afshari, P.; Goodin, M.; Horner, M., Assessing Computational Model Credibility Using a Risk-Based Framework: Application to Hemolysis in Centrifugal Blood Pumps. *ASAIO journal (American Society for Artificial Internal Organs : 1992)* **2019,** 65, (4), 349-360.

103. Marino, S.; Hogue, I. B.; Ray, C. J.; Kirschner, D. E., A methodology for performing global uncertainty and sensitivity analysis in systems biology. *J Theor Biol* **2008,** 254, (1), 178-196.